

Accepted Manuscript

The role of disulfide-bridge on the activities of H-shape gemini-like cationic lipid based siRNA delivery

Xiao-Fei Ma, Jing Sun, Chong Qiu, Yi-Fan Wu, Yi Zheng, Min-Zhi Yu, Xi-Wei Pei, Lin Wei, Yu-Jie Niu, Wen-Hao Pang, Zhen-Jun Yang, Jian-Cheng Wang, Qiang Zhang

PII: S0168-3659(16)30330-3
DOI: doi: [10.1016/j.jconrel.2016.05.051](https://doi.org/10.1016/j.jconrel.2016.05.051)
Reference: COREL 8294

To appear in: *Journal of Controlled Release*

Received date: 8 September 2015
Revised date: 17 May 2016
Accepted date: 23 May 2016

Please cite this article as: Xiao-Fei Ma, Jing Sun, Chong Qiu, Yi-Fan Wu, Yi Zheng, Min-Zhi Yu, Xi-Wei Pei, Lin Wei, Yu-Jie Niu, Wen-Hao Pang, Zhen-Jun Yang, Jian-Cheng Wang, Qiang Zhang, The role of disulfide-bridge on the activities of H-shape gemini-like cationic lipid based siRNA delivery, *Journal of Controlled Release* (2016), doi: [10.1016/j.jconrel.2016.05.051](https://doi.org/10.1016/j.jconrel.2016.05.051)

This is a PDF file of an unedited manuscript that has been accepted for publication. As a service to our customers we are providing this early version of the manuscript. The manuscript will undergo copyediting, typesetting, and review of the resulting proof before it is published in its final form. Please note that during the production process errors may be discovered which could affect the content, and all legal disclaimers that apply to the journal pertain.



The role of disulfide-bridge on the activities of H-shape gemini-like cationic lipid based siRNA delivery

Xiao-Fei Ma¹, Jing Sun¹, Chong Qiu¹, Yi-Fan Wu, Yi Zheng, Min-Zhi Yu, Xi-Wei Pei, Lin Wei, Yu-Jie Niu, Wen-Hao Pang, Zhen-Jun Yang*, Jian-Cheng Wang**, Qiang Zhang

State Key Laboratory of Natural and Biomimetic Drugs, School of Pharmaceutical Sciences, Peking University, Beijing, 38 xueyuan Road, 100191, China.

*Corresponding Author:

Jian-Cheng Wang, Ph.D, Tel/Fax: 86-10-82805932, Email: wang-jc@bjmu.edu.cn; & Zhen-Jun Yang, Ph.D, Tel/Fax: 86-10-82802503, Email: yangzj@bjmu.edu.cn;

¹These authors equally contributed to this work.

Abstract

In our previous study, a H-shape gemini-like cationic lipid (ssGLCL, formerly named as CLD), composed of two hydrophilic lysine heads and two hydrophobic oleyl alcohol tails with a bridge of the redox-active disulfide-bond, had been synthesized and used as a nanocarrier for delivering small interfering RNAs (siRNAs) into cells. In order to further elucidate the role of disulfide (-S-S-) bridge on the activity of ssGLCL based siRNA delivery, a comparable ccGLCL bridged with a non-reducible carbon-carbon bond was synthesized and used as control in this study. Both two H-shape GLCL molecules could individually self-assemble into cationic nanoparticles in water phase and complex with negatively-charged siRNA into nanoplexes with particle size of ~ 200 nm and zeta potential of ~ +30 mV, and exhibit effective siRNA delivery both *in vitro* and *in vivo*. Investigation of internalization pathway displayed that both ssGLCL/siRNA and ccGLCL/siRNA nanoplexes were predominantly internalized into MCF-7 cells by the clathrin-mediated endocytosis pattern. Although a lower cellular uptake of siRNA was found in the human breast cancer MCF-7 cells, the ssGLCL/siRNA nanoplexes could exhibit similar or even stronger down-regulation effects on the targeted EGFR mRNA and protein in MCF-7 cells when compared to the ccGLCL/siRNA nanoplexes. Furthermore, mechanistic study showed that the enhanced down-regulation effects of ssGLCL/siRNA nanoplexes on targeted mRNA and protein were probably attributed to the increased release of siRNA from lysosomes to cytoplasm following the cleavage of redox-active disulfide-bridge in ssGLCL. Therefore, we believed that the redox-active H-shape ssGLCL could be a potential nanocarrier towards improving siRNA delivery.

Keywords: siRNA delivery, gemini-like lipid, disulfide bond, biodegradation, nanocarrier.

1. Introduction.

Nowadays small interference RNA (siRNA) is regarded as a significant potential therapeutic agent for diverse diseases, especially tumors [1-4]. However, its inherent defects

impede the further clinic progress [5-7]. Hence, a lot of nanocarrier-based delivery systems have emerged immensely for relieving this dilemma [8-10]. Therein, cationic liposomes have been deemed as the most promising gene vectors for their efficient transfection and facile formulation [11, 12].

As one distinct representative, gemini-like cationic lipids (GLCLs) have particular superiority and evoke interest in biological and biomedical applications [13, 14]. These structures of H-shape or X-shape GLCLs are generally composed of three basic ingredients: two cationic heads, two aliphatic tail chains and a rigid or flexible linker [15, 16]. These distinctive properties endowed GLCLs not only the higher encapsulation efficiency but also the lower cytotoxicity than those of corresponding monomeric lipids, which displayed advantages for delivery DNA and antisense oligonucleotide (AS-ODN) drugs [17-19]. In our previous studies [20], a novel H-shape gemini-like cationic lipid (**ssGLCL**, formerly named as **CLD**), composed of two hydrophilic lysine heads and two hydrophobic oleyl alcohol tails linked with disulfide (-S-S-) bridge, had been synthesized and used as a nanocarrier for siRNA delivery.

In recent years, the concept of “environment-response” was fused in the design of siRNA delivery systems [21, 22]. These stimuli-responsive features (such as pH [23], enzyme [24], redox [25], and hypoxia [26] etc.) promote the disassembly of nanoplexes and increase the release of siRNA from endosomes or lysosomes, consequently improving gene silencing effects on targeted mRNA. During the past years, disulfide-bond structures were embedded into multiple delivery systems based on the intracellular redox environment [27-32]. The redox imbalance between extra- and intracellular environments in tumor tissues endowed it biodegradable characteristics in the presence of excess reductive substances in cytoplasm, thus mediating redox-degradation assisted release of gene drugs and improving transfection efficacy.

Our previous study have demonstrated that the siRNA targeting MEK1 mRNA formulated with **ssGLCLs** into lipoplexes could exhibit an effective gene silencing of MEK1 expression [20]. However, there were still some important mechanistic issues need be further investigated: i) the cationic nanoparticles self-assembled with amphiphilic **ssGLCL** molecules would possess a higher capacity for siRNA package and protection; ii) the prepared **ssGLCL**/siRNA nanoplexes would exhibit a lower cytotoxicity; iii) enhanced silencing on targeted mRNA would be obtained by a redox-assisted siRNA releasing from lysosomes to cytoplasm attributed to the cleavage of disulfide-bridge in H-shape **ssGLCL**.

To elucidate the mechanisms of the role of disulfide-bridge on the activities of H-shape **ssGLCL** based siRNA delivery, the analogous of H-shape gemini-like cationic lipid (**ccGLCL**) bridged with a non-reducible carbon-carbon bond, instead of disulfide-bridge, were also synthesized as an important reference. In addition, monomeric lipid units (named as **sGLCL**) were also synthesized as the mimic residue after cleavage of H-shape **ssGLCL**.

2. Materials and methods.

2.1 Materials and Cell Lines

1-Ethyl-3-(3-dimethylaminopropyl)-carbodiimide hydrochloride (**EDCI**), 4-dimethylaminopyridine (**DMAP**), N-Hydroxybenzotriazole (**HOBt**) and **L-2**, 6-diaminopimelic acid

were obtained from J&K Scientific Ltd. (Beijing, China). Boc-Lys(Boc)-OH, alanine, cysteine, oleyl alcohol, and Boc₂O were purchased from GL Biochem Co., Ltd. (Shanghai, China). Lipofectamine2000, OPTI-MEM, and LysoTracker Red DND-99 were purchased from Invitrogen (NY, USA); Agarose was obtained from GENE COMPANY (Hong Kong, China); Hoechst 33258 was purchased from Molecular Probes Inc. (Oregon, USA); sulforhodamine B (SRB) was purchased from Sigma Aldrich. Co. (St. Louis, MO). Anti-EGFR siRNA (sense strand: 5'-AGGAAUUAAGAGAAGCAACAUDtT-3'; antisense strand: 5'-AUGUUGCUUCUCUUAUUCUdT-3', named as siEGFR), Anti-VEGF siRNA (sense strand: GGAGUACCCUGAUGAGAUCdT, antisense strand: 5'-GAUCUCAUCAGGGUACUCCdT-3', named as siVEGF), Anti-GFP siRNA (sense strand: 5'-GGCUACGUCCAGGAGCGCACC-3'; antisense strand: 5'-UGCGCUCC UGGACGUAGCCUU, named as siGFP), negative control siRNA (sense strand: 5'-UUC UCC GAA CGU GUC ACG UTT-3'; antisense strand: 5'-ACG UGA CAC GUU CGG AGA ATT-3'. named as siNC) and fluorescein-labeled siRNA (5'end of the sense strand, FAM-siRNA) were synthesized and purified with HPLC by GenePharma Co. Ltd (Shanghai, China). Human breast cancer MCF-7 cells, human cervical cancer HeLa cells and those who can express GFP (Green Fluorescence Protein) stably (GFP-HeLa cell line) were obtained from the Institute of Basic Medical Science, Chinese Academy of Medical Sciences (Beijing, China). The cells were cultured in RPMI-1640 medium (Macgene, Beijing, China) supplemented with 10% fetal bovine serum (FBS), 100 units/mL penicillin and 100 mg/mL streptomycin at 37°C in a humidified atmosphere containing 5% CO₂. The cells for all experiments were in the logarithmic phase of growth.

2.2 Synthesis of GLCLs Materials.

Three novel GLCLs materials were synthesized in a similar scheme. The synthetic route of **ssGLCL** material was described here as the representative procedure. In brief, the Boc-protected cystine **2** was firstly prepared and then esterificated with oleyl alcohol under the coupling reagents EDC and DMAP to obtain intermediate **3** as colorless gel. Compound **3** was deprotected by TFA to produce compound **4** as yellow grease. Intermediate **5** was formed as colorless wax in amidation between compound **4** and Boc-Lys (Boc)-OH under activator EDCI and HOBt. Then compound **5** was deprotected again and salified by HCl gas to obtain the **ssGLCL** (compound **6**) as a white solid. All products were confirmed by ¹H nuclear magnetic resonance (AVANCE III, 400 MHz, Bruker, Billerica, MA) and ESI-MS spectrometry (VG Scienta, England). The total synthetic yield was 67.6% and the detailed processing was seen in supplementary information.

2.3 Preparation and Characterization of GLCL/siRNA Nanoplexes.

GLCL nanoparticles were prepared using thin film hydration method. Briefly, GLCL materials were dissolved into methanol in a flask with appropriate concentration, and then organic solvent was removed by rotary evaporation method at 37°C for 15 min. The formed film was hydrated by 5% glucose solution pretreated with diethyl pyrocarbonate (DEPC) and sterilization at 60°C, subsequently sonicated at 70°C for 40 min. As a result, GLCL nanoparticles were obtained. To form the GLCL/siRNA nanoplexes, the GLCL nanoparticles and siRNA were mixed together with N/P = 10/1 or other ratios, and the nanoplexes were

incubated at 37°C for 20 min, and then diluted to certain concentration for use. The particle sizes and zeta potentials of nanoplexes were measured at 25°C using dynamic light scattering (Malvern Zetasizer Nano ZS, Malvern, UK). The morphology of nanoplexes was observed by transmission electron microscope (TEM, JEOL, Japan) and atomic force microscope (AFM, Veeco Metrology, USA).

2.4 Gel Retardation Assay.

Various GLCL/siRNA nanoplexes were prepared at different N/P ratios, the final siRNA concentration was fixed at 1 µM. Then these prepared nanoplexes were tackled with loading buffer and electrophoresed with 1% agarose gel containing 0.5 mg/mL Exred (a special luminant dye for siRNA staining). Electrophoresis was performed at 80 mV for 3 min, subsequently 100 mV for 10 min, and these resulting gels were photographed under UV-illumination. Free siRNA was used as the control.

2.5 Cytotoxicity Assay.

In vitro cytotoxicity of GLCL nanoparticles on MCF-7 cells was performed by sulforhodamine B (SRB) assay. Briefly, MCF-7 cells were seeded in 96-well plates at a density of 5000 cells per well. After 24 h proliferation, cells were treated with 200 µL OPTI-MEM containing serial concentrations of each nanoparticle. The medium was replaced by RPMI-1640 medium containing 10% FBS after 4h incubation, and then followed by another 48 h incubation. Removed the culture medium carefully, fixed cellular protein by the addition of 100 µL of 10% TCA (trichloroacetic acid) at 4°C for 1 h, the 96-well plates were then washed with deionized water for five cycles and air dried. The SRB solution (200 µL) was added into each well and allowed staining for a 30 min in dark condition. Then, the SRB solution was removed, and plates were washed with 1% acetic acid for five times. After air-dried, 100 µL of 10 mM Tris base solution was added into each well to solubilize the protein-bound dye on a gyratory shaker for 30 min. Absorbance values were read on a microplate reader at the wavelength of 540 nm. The cell viability (%) was calculated according to the following formula: Cell viability (%) = [OD₅₄₀ (sample)/OD₅₄₀ (control)] × 100 %, where OD₅₄₀ (sample) is the absorbance from the cells treated with various nanoparticles and OD₅₄₀ (control) is that from the cells treated with 5% glucose.

2.6 Hemolysis Assay.

Various GLCL nanoparticles were separately diluted to a final concentration of 0.96 mg/mL with 5% glucose. Erythrocytes (RBC) were isolated from rat blood by centrifugation at 1500 g for 10 min at 4°C and were washed with physiological saline solution three times at the same condition as above. The cell pellet was resuspended into a 2% (v/v) erythrocyte suspension with pre-chilled PBS (0.1 M, pH = 7.4), and then the erythrocyte suspensions (180 µL) were loaded in each well of 96-well plates. Aliquot 20 µL of nanoparticle suspensions was added into each well of the plates. Each sample was separated in two groups of erythrocyte suspension without or with DTT reagent (final concentration was set as 10 mM). The 5% glucose solution was used as a negative control, and Triton X-100 (1%, v/v) was used as a positive control. At predetermined time points, each sample was centrifuged and the supernatant was transferred to a new plate, and the absorbance was measured at 540 nm using

a microplate reader.

2.7 Cellular Uptake of GLCL/siRNA Nanoplexes.

MCF-7 cells and HeLa cells (3×10^5 per well) were seeded in six-well plates. After 24 h proliferation, various formulations containing FAM-siRNA with different N/P ratios at the fixed final concentration of 100 nM were exposed to cells and incubated for an additional 4 h at 37 °C. After incubation, the cells were harvested and washed three times with pre-cooled PBS solution and the uptake of FAM-siRNA was detected by a FACS Calibur flow cytometer (Becton Dickinson, San Jose, CA, USA) immediately. Confocal microscopy was also used to observe the internalization efficacy of GLCL/siRNA nanoplexes. After transfected for 4 h, the cells were washed three times with PBS followed by fixation with 4% paraformaldehyde for 15 min at room temperature. Then, F-actin and nucleus were individually stained by rhodamine labeled phalloidin and Hoechst 33258 as the manufacturer's instructions. The cells were visualized under a Leica TCS SP5 confocal fluorescence microscope (Leica Microsystems, Heidelberg, Germany).

2.8 Endocytic Mechanism of GLCL/siRNA Nanoplexes

HeLa or MCF-7 Cells were seeded in 12-well plates at 2×10^5 cells/well for 24 hours before transfection. Transfections were performed with the presence of inhibitors in cell culture medium (50 µg/mL genistein, 10 g/mL chlorpromazine, 0.25 mM amiloride). Firstly, prior to transfection, cell culture medium was replaced with serum-free medium containing the desired inhibitors for 30 minutes. Then, various FAM-siRNA loaded formulations with N/P = 10/1 at the final siRNA concentration of 100 nM were exposed to cells and incubated for an additional 4 hours at 37°C. In the process of incubation, the concentration of inhibitors was consistent with the pre-treatment. After incubation, the cells were harvested and washed with pre-cooled PBS solution three times and the intracellular fluorescence intensities were detected by a FACS Calibur flow cytometer (Becton Dickinson, San Jose, CA, USA) immediately.

Confocal microscopy was also used to observe the co-localization of channel markers with fluorescence-labeled GLCL/siRNA nanoplexes. MCF-7 Cells were seeded in confocal dishes (2×10^5 cells/dish) for 24 hours prior to transfection. Then, various formulations containing Cy5-siRNA with N/P = 10/1 at the final concentration of 200 nM were exposed to cells and incubated for an additional 2 hours at 37°C. Before the end of incubation, transferrin labeled with Alexa Fluor-488 (10 µg/mL, 30 min), Cholera Toxin Subunit B labeled with Alexa Fluor-488 (2 µg/mL, 30 min) and Dextran labeled with FITC (1 mg/mL, 1 hour) were dropped into the culture medium respectively. After treated, the cells were washed with PBS three times followed by fixation with 4% paraformaldehyde for 15 min and cell punching with 0.1% Triton-PBS for 1 min at room temperature. Then, F-actin and nucleus were individually stained by rhodamine labeled phalloidin (1 U/mL, 10 min) and Hoechst 33258 (5 µg/mL, 10 min) according to the manufacturer's instructions. Cells were visualized by a Leica TCS SP8 confocal fluorescence microscope (Leica Microsystems, Heidelberg, Germany).

2.9 Intracellular Distribution of GLCL/siRNA Nanoplexes.

MCF-7 cells (2×10^5 cells per well) were seeded into confocal dishes. After 24 hours

incubation, the GLCL/FAM-siRNA nanoplexes suspension (the final siRNA concentration equal to 100 nM, dispersed in OPTI-MEM medium) was added into each dish for different time periods. At the end of transfection, LysoTracker Red (Invitrogen, Carlsbad, USA) (50 nM) was added in cell culture medium and incubated for 30 min at 37°C for staining endosomes/lysosomes. Then the cells were washed with PBS for three times, and fixed in 4% paraformaldehyde. Intracellular fluorescence distribution of FAM-siRNA was observed with a Leica SP 5 confocal microscope (Leica Microsystems, Heidelberg, Germany).

2.10 *In vitro* Gene Silencing Effects.

The levels of mRNA and protein in the cells treated with different nanoparticles (N/P = 10/1, final siRNA concentration were 100 nM) were analyzed by RT-PCR and western blot technologies. To detect relative EGFR mRNA expression, MCF-7 cells were treated similarly as the process in *Cellular Uptake Section*, except for the usage of siEGFR. Then cells were incubated by another 24 h of incubation. Total RNA was extracted using TRIOL® reagent method and reverse transcribed with ReverTra Ace qPCR RT Kit (TOYOBO, Japan). The resulting cDNAs were used for PCR using THUNDERBIRD qPCR Mix (TOYOBO, Japan) in triplicates. PCR and data collection were performed on Real-Time PCR amplifier (MX3005P, Stratagene, USA). All quantitation were normalized to an endogenous control GAPDH. The relative quantitation value for each target gene compared to the calibrator for that target is expressed as $2^{-(Ct-Cc)}$ (Ct and Cc are the mean threshold cycle differences after normalizing to GAPDH). For western blot analysis of EGFR protein, similar cell culture and treatments were performed as above described. After transfection for 48 h, the cells were washed with pre-cooled PBS and then resuspended in 100 mL RIPA lysis buffer supplemented with 1% proteinase inhibitor cocktail. The cell lysates were incubated on ice for 30 min and vortexed every 10 min. The total protein was gathered by centrifugation at 12,000 g for 5 min and their concentration was determined with BCA protein assay kit. Total protein (30 mg) was loaded on 10% sodium dodecyl sulfate polyacrylamide gel and electrophoresized at 80 mV for 30 min and 120 mV for 2 h. Then the proteins were transferred to Polyvinylidene Fluoride (PVDF) membranes at 200 mA for 90 min then blocked with 5% skimmed milk on a horizontal shaker for 1h. The membranes were incubated with the 1:500 EGFR monoclonal antibody (Santa Cruz Biotechnology) overnight at 4 °C, followed by incubation with HRP-conjugated goat anti-rabbit antibodies (1:15,000; Zhongshan Golden-Bridge Co. Ltd., Beijing, China) at room temperature for 2 h. Finally, the membranes were exposed using a Bio-rad ChemiDoc XRS System. β -Actin was used as endogenous control. In addition, the fluorescence intensities of GFP in HeLa cells (GFP-HeLa cell line) treated with different nanoplexes were detected. For GFP detection, similar cell culture and treatments were performed as above described except for the usage of siGFP. After 48 h incubation, the cells were harvested and washed three times with pre-cooled PBS solution and the fluorescence intensity of GFP was detected by a FACS Calibur flow cytometer (Becton Dickinson, San Jose, CA, USA) immediately. Another important VEGF protein in MCF-7 cell culture medium was also analyzed using a Human VEGF immunoassay kit (Raybiotech, USA). Similar cell culture and treatments were performed as above described except for the usage of siVEGF. The final concentrations of siVEGF were 30, 50, 100 nM. After 4 h incubation, the OPTI-MEM medium was replaced with fresh complete medium, followed by 8 h incubation.

After that, the medium was changed to fresh complete medium and incubated for additional 16 h. Finally, the medium was collected and analyzed using a human VEGF immunoassay kit (RayBiotech, USA) according to the manufacturer's instructions. The untreated cells and the cells treated with Lipofectamine2000 were used as negative and positive controls, respectively.

2.11 *In Vivo Anti-Tumor Study.*

Six-week-old female Balb/c nude mice were housed in an air-conditioned room. All care and handling of animals was performed with the approval of Institutional Authority for Laboratory Animal Care of Peking University. MCF-7 cells (2×10^6 cells of each injection) were inoculated subcutaneously in the right flank of each Balb/c nude mouse. Tumor growth was monitored by measuring the tumors perpendicular diameter using a caliper. Estimated tumor volume was calculated using the formula: $\text{volume (mm}^3\text{)} = (\text{length} \times \text{width}^2)/2$. The treatment was started at 7th day post-implantation when the tumor volume reached approximately 80 mm³. The female balb/c nude mice xenografted MCF-7 tumors were randomly divided into five groups and injected intratumorally with different siRNA formulations at a dose of 1 mg/kg every other day for four times. 5% glucose was used as control. Body weight and tumor size of each mouse were also measured every day. Two days after the last injection, the tumor tissues were excised for further investigation.

2.12 *Immunofluorescence Detection of EGFR Protein in Tumor Tissue.*

After sacrifice, tumor tissues collected from the nude mice were immediately embedded in Tissue-Tek OCT (Sakura Finetek, Tokyo, Japan), frozen rapidly and subsequently cut into 5-mm cryo-sections. Sections of tumor tissues were fixed in pre-cooled acetone for 10 min at 4°C, followed by incubated with 1% BSA for 30 min and subsequently with 1:50 anti-EGFR rabbit monoclonal antibody (Abcam, Cambridge, United Kingdom) overnight at 4°C. After being washed with PBS, the sections were treated with a 1:100 dilution of FITC-conjugated goat anti-rabbit IgG (Zhongshan Golden-Bridge Co. Ltd., Beijing, China) at 37°C for 1 hour. After staining of the nucleus with Hoechst 33258 (2 mg/mL) for 25 min, the cryosections were observed by Leica SP8 confocal microscopy.

2.13 *Statistical Analysis*

For statistical analysis between two groups, Student's t-test for independent means was applied. The differences between any two groups out of several groups were analyzed by one-way analysis of variance (ANOVA) followed by LSD multiple comparisons. Statistical analysis was performed with the SPSS software (Version 16.0, SPSS Inc, Chicago).

3. Results

3.1 *Synthesis and Structural Confirmation of GLCLs.*

The representative synthesis procedure of GLCLs materials was shown in **Scheme 1**.

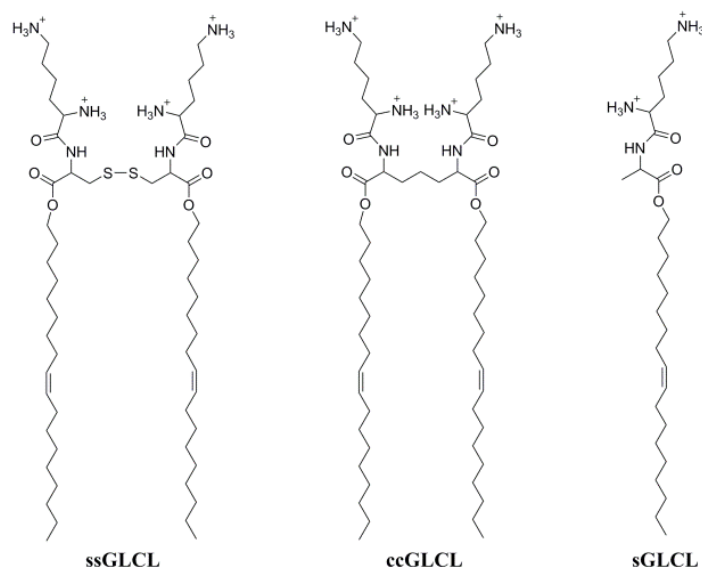


Figure 1. Structures of ssGLCL/ccGLCL/sGLCL materials.

3.2 Characterization of GLCL/siRNA Nanoplexes.

As seen from **Table 1**, all GLCL nanoparticles could complex with siRNA effectively and form the uniform nanoplexes at N/P = 10/1 with a mean size around 200 nm. The ssGLCL/siRNA nanoplexes and the ccGLCL/siRNA nanoplexes shared similar zeta potentials of 30.5 ± 1.8 mV and 33.3 ± 1.5 mV, respectively. However, zeta potential of sGLCL/siRNA nanoplexes was only 13.9 ± 1.5 mV, which was significantly lower than those of the other nanoplexes.

Table 1. Characteristics of various nanoplexes

Nanoplexes	Particle size (d, nm)	Polydispersity index(PDI)	Zeta potential (mV)
ssGLCL/siRNA	232.1 \pm 4.2	0.14 \pm 0.067	30.5 \pm 1.8
ccGLCL/siRNA	231.7 \pm 30.1	0.27 \pm 0.102	33.3 \pm 1.5
sGLCL/siRNA	199.0 \pm 4.7	0.31 \pm 0.034	13.9 \pm 1.5

The morphology was observed by TEM and AFM. It showed that GLCLs nanoparticles and corresponding siRNA nanoplexes were uniform spherical vesicles without obvious aggregation (**Figure 2A and B**). Compared to GLCL nanoparticles, these GLCL/siRNA nanoplexes were observed as darker blots in TEM images and smaller ones in AFM images, which indicated that GLCLs nanoparticles and siRNAs were compacted together more tightly due to the electrostatic interaction.

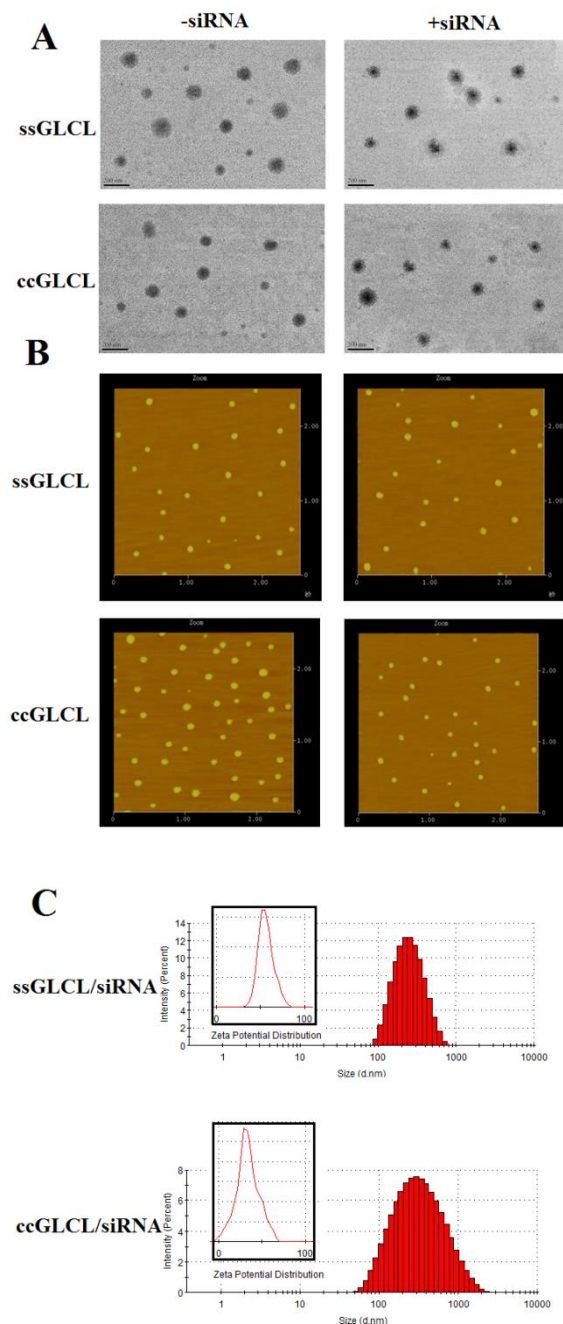


Figure 2. Characterization of the prepared nanoparticles. TEM (A) and AFM (B) images of GLCL nanoparticles and their siRNA complexes. Size and zeta potential of nanoplexes detected by DLS (C).

The results of gel retardation assay further confirmed that siRNA could be completely compacted by all cationic GLCL nanoparticles at an N/P ratio as low as 3/1, with no difference among these nanoplexes (**Figure 3A**). Cytotoxicity assay (**Figure 3B**) showed that there were no significant difference between **ssGLCL** and **ccGLCL** nanoparticles, however, the nanoparticles composed of the monomeric lipid **sGLCL** presented markedly cytotoxicity to MCF-7 cells than other two H-shape GLCLs nanoparticles.

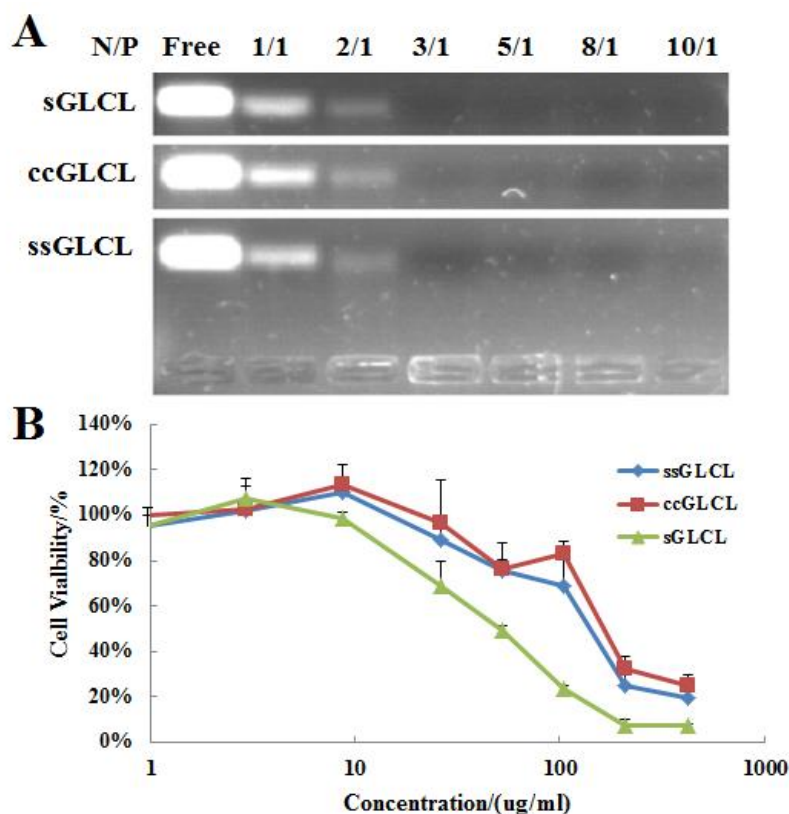


Figure 3. Gel retardation assay for various nanoplexes at different N/P ratios (A). Cytotoxicity of various GLCL nanoparticles in MCF-7 cells (B).

3.3 Cellular Uptake of GLCL/siRNA Nanoplexes.

With cellular uptake of siRNA, higher fluorescence intensities were found in cells after 4 h incubation with various GLCL/FAM-siRNA nanoplexes with different N/P ratios (**Figure 4A**). In MCF-7 cells, **ccGLCL**/FAM-siRNA group showed much higher fluorescence intensity than **ssGLCL**/FAM-siRNA at almost all N/P ratios. When the ratio of N/P up to 10/1 or more, a significantly higher cellular uptake of siRNA was found in the **ccGLCL**/FAM-siRNA nanoplexes than that of lipofectamine2000. In CLSM images (**Figure 4B**), **ccGLCL** group displayed a higher green fluorescence intensity than **ssGLCL** group. During observation by CLSM, the rhodamine-labeled phalloidin (red fluorescence) was used to display the cytoskeleton. Surprisingly, much more incomplete cell membrane was observed in MCF-7 cells after 4 h incubation with **ccGLCL**/FAM-siRNA nanoplexes, while the smooth and intact cell membrane was still observed in the **ssGLCL**/FAM-siRNA group. Interestingly, this phenomenon was hardly found in HeLa cells when these two GLCL/siRNA nanoplexes were incubated. Therefore, the N/P ratio of 10/1 was selected as an optimal ratio for both of MCF-7 and HeLa cells in the following experiments.

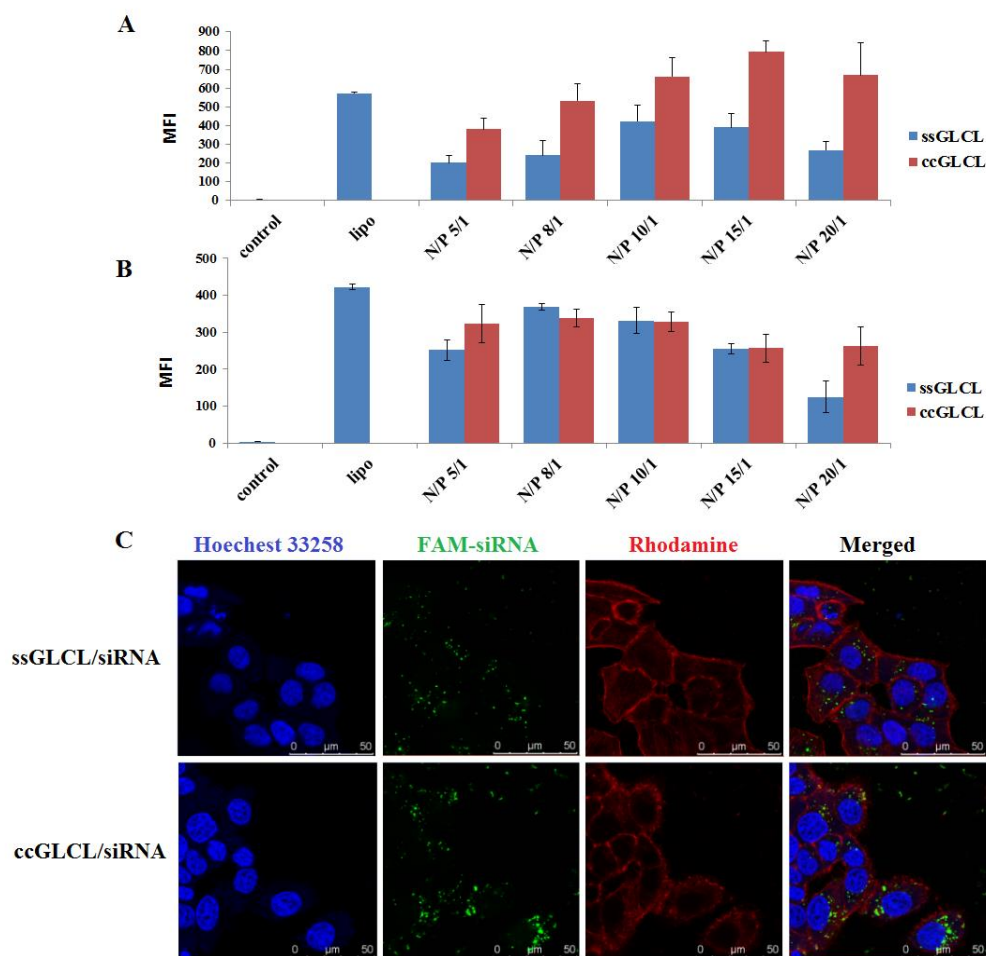


Figure 4. Cellular uptake of various nanoplexes in MCF-7 cells (A) and HeLa cells (B). The intracellular fluorescence intensities were detected by flow cytometric after 4h incubation with different nanoplexes with different N/P ratios. The data was shown as mean \pm SD ($n = 3$). (C) Confocal laser scanning microscope images of MCF-7 after 4h incubation with ssGLCL/siRNA nanoplexes and ccGLCL/siRNA nanoplexes with a final siRNA concentration of 100 nM at N/P = 10/1. The Rhodamine-labeled phalloidin (red) was used to show the cytoskeleton and Hoechst 33258 (blue) for nucleus.

3.4 Endocytic Mechanism of GLCL/siRNA Nanoplexes

Endocytosis mechanisms were generally divided into four classes: clathrin-mediated endocytosis (CME), caveolae-mediated endocytosis (CvME), macropinocytosis and CME/CvME-independent endocytosis. In our study, two approaches were performed to elaborate the endocytosis pathways of the GLCL/siRNA nanoplexes: i) Specific blocking agents were used to block internalization channels. Amiloride, chlorpromazine (CPZ), genistein and NaN_3 are known as the inhibitors of macropinocytosis, CME-mediated endocytosis, CvME-mediated endocytosis and ATP-dependent endocytosis respectively. The changes of intracellular fluorescence intensities were detected by flow cytometry; ii) Specific markers were used to indicate the co-localization of endocytosis pathway of the fluorescence-labeled nanoplexes and the fluorescence distribution was detected by CLSM

image.

As shown in **Figure 5A₁**, the intracellular fluorescence intensities of **ssGLCL/siRNA** nanoplexes were about 25% decrease induced by amiloride, CPZ and NaN₃ respectively; For **ccGLCL/siRNA** nanoplexes, the fluorescence intensity decreased by CPZ was about 50%. In **Figure 5B₁**, a significant reduction of fluorescence intensity (~ 50%) was observed in both **ssGLCL/siRNA** and **ccGLCL/siRNA** nanoplexes when they were blocked with genistein and NaN₃. Seen from the results of various channel rates shown in **Figure 5A₂** and **5B₂**, both **ssGLCL/siRNA** and **ccGLCL/siRNA** nanoplexes were internalized into MCF-7 cells or HeLa cells predominantly through the CME-mediated endocytosis pathway (50% ~ 70%).

In CLSM images, the fluorescence-labeled transferrin, cholera toxin B and dextran (green color) were used as the channel markers to trace intracellular trafficking routes of GLCL/siRNA nanoplexes (Cy5-labeled siRNA, red) by co-localization observation. As shown in **Figure 5C**, both **ssGLCL/siRNA** nanoplexes and **ccGLCL/siRNA** nanoplexes were mainly co-localized with transferrin (yellow color); while no obvious co-localization were found between **ssGLCL/siRNA** nanoplexes and CT-B, as well as seen from the co-localization between **ccGLCL/siRNA** nanoplexes and dextran. These results were consistency with those results detected by FCM (**Figure 5A**).

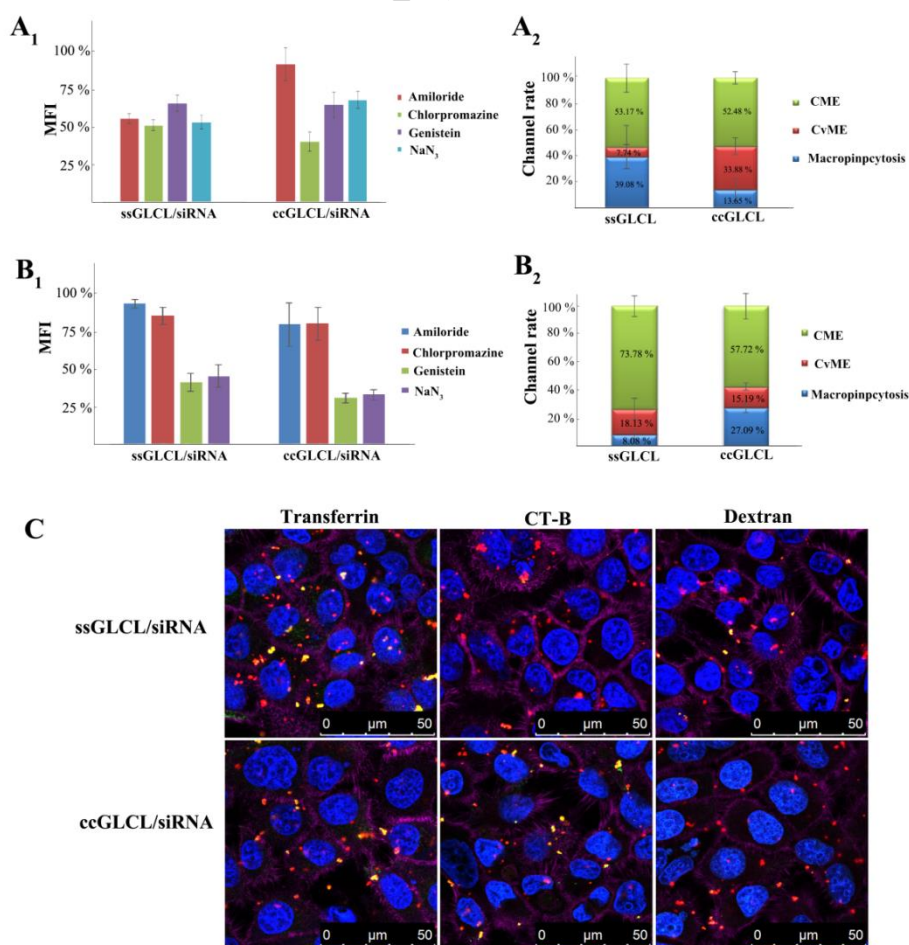


Figure 5. Internalization of various nanoplexes after treated with different inhibitors in MCF-7 cells (A) and HeLa cells (B). The intracellular fluorescence intensities were detected

by flow cytometry after 4 h incubation. The mock (100%) was the fluorescence intensity of various nanoplexes without inhibitors. The data was shown as mean \pm SD ($n = 3$). (C) Internalization pathways of various nanoplexes in MCF-7 cells by confocal microscopy. Hoechst 33258 (Blue) and rhodamine-labeled phalloidin (Purple) were used to show the nucleus and membrane respectively. The final concentration of Cy5-labeled siRNA (Red) was 100 nM.

3.5 Evaluation of Disulfide-Bond Function.

Firstly, the cleavage of disulfide-bond in **ssGLCL** was investigated by comparing the different hemolysis effects of GLCLs on red cells with or without DTT addition. As seen from **Figure 6A**, before the addition of DTT, only **sGLCL** nanoparticles showed significant hemolysis effects (about 65%), while there were no difference on the other groups compared with 5% glucose, which was used as a negative control. However, a significant hemolysis effect was found in **ssGLCL** nanoparticles (up to almost 40%) after the addition of DTT reagent, while **ccGLCL** still did not show any hemolysis effect. This difference between **ssGLCL** and **ccGLCL** nanoparticles may indicate the special property of disulfide-bond under the reductive condition.

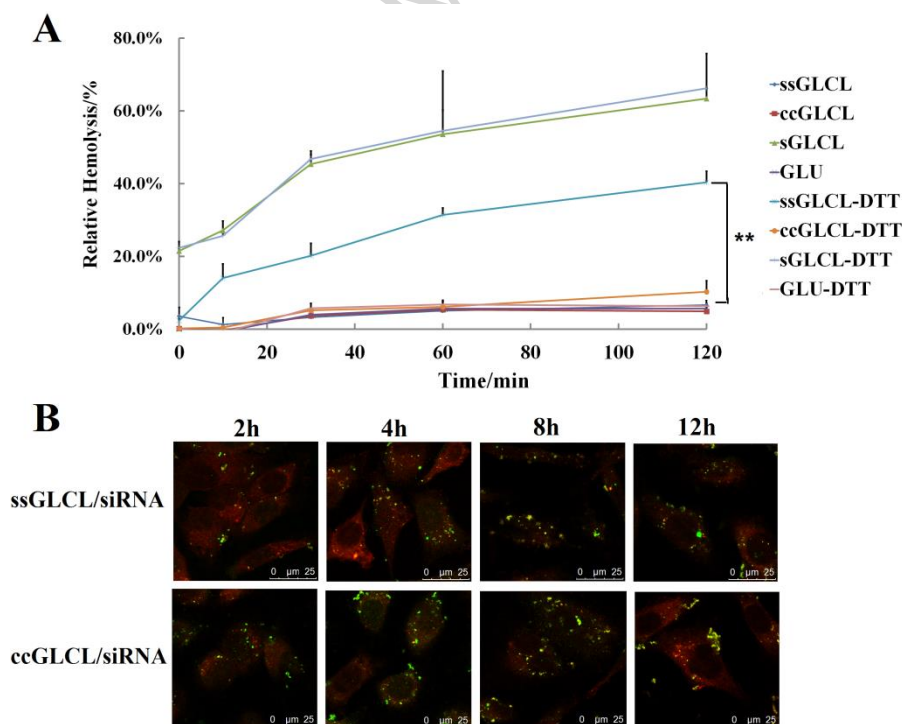


Figure 6. A. Relative hemolysis effects of different nanoplexes in the absence/presence of DTT with different incubation time at 37°C. Data was shown as mean \pm SD ($n=3$). ** $p < 0.01$. B. CLSM images of MCF-7 cells after incubated with various GLCL/siRNA nanoplexes at N/P = 10/1 for different time periods. The LysoTracker Red DND-99 (red) was used to show the endosomes/lysosomes. The final FAM-siRNA concentration is 100 nM.

Secondly, the endosome/lysosome escape of **ssGLCL** and **ccGLCL** in MCF-7 cells were evaluated by CLSM imaging to estimate that whether the cleavage of disulfide-bond in

lysosomes would promote the release of siRNA from **ssGLCL** nanoplexes into cytoplasm, which resulted in higher gene silencing activities. As seen from **Figure 6B**, at 4 h time point, **ssGLCL/FAM-siRNA** and **ccGLCL/FAM-siRNA** nanoplexes were all internalized into cytoplasm as green discrete dots. As time went by, the co-localization of nanoplexes and endosomes/lysosomes was gradually presented as yellow dots. At 8 h point (**Figure 7A**), either in **ssGLCL** group or in **ccGLCL** group, more and more yellow dots appeared in cytoplasm, that meant the similar endosomal/lysosomal internalization pathway was happened for these two nanoplexes. More interesting, in **ssGLCL/FAM-siRNA** group, a lot of green dots appeared again in cytoplasm at 12 h point, that meant large percentage of green-fluorescence labeled siRNA was released from lysosomes into cytoplasm. In contrast, there were many yellow dots still displayed in cytoplasm in **ccGLCL/FAM-siRNA** group. This change was further confirmed by the quantitative analysis of Pearson's correlation coefficient. As seen in **Figure 7B**, it was shown that the Pearson's correlation coefficient decreased from 0.7007 (at 8 h point) to 0.4643 (at 12 h point) in **ssGLCL** group, while the **ccGLCL** group changed from 0.7067 (at 8 h point) to 0.7981(at 12 h point). These results suggested that the disulfide cleavage of **ssGLCL** under the reductive condition played an important role for the release of siRNA from lysosome escape, which was consistent with the results of hemolysis assay in **Figure 6A**.

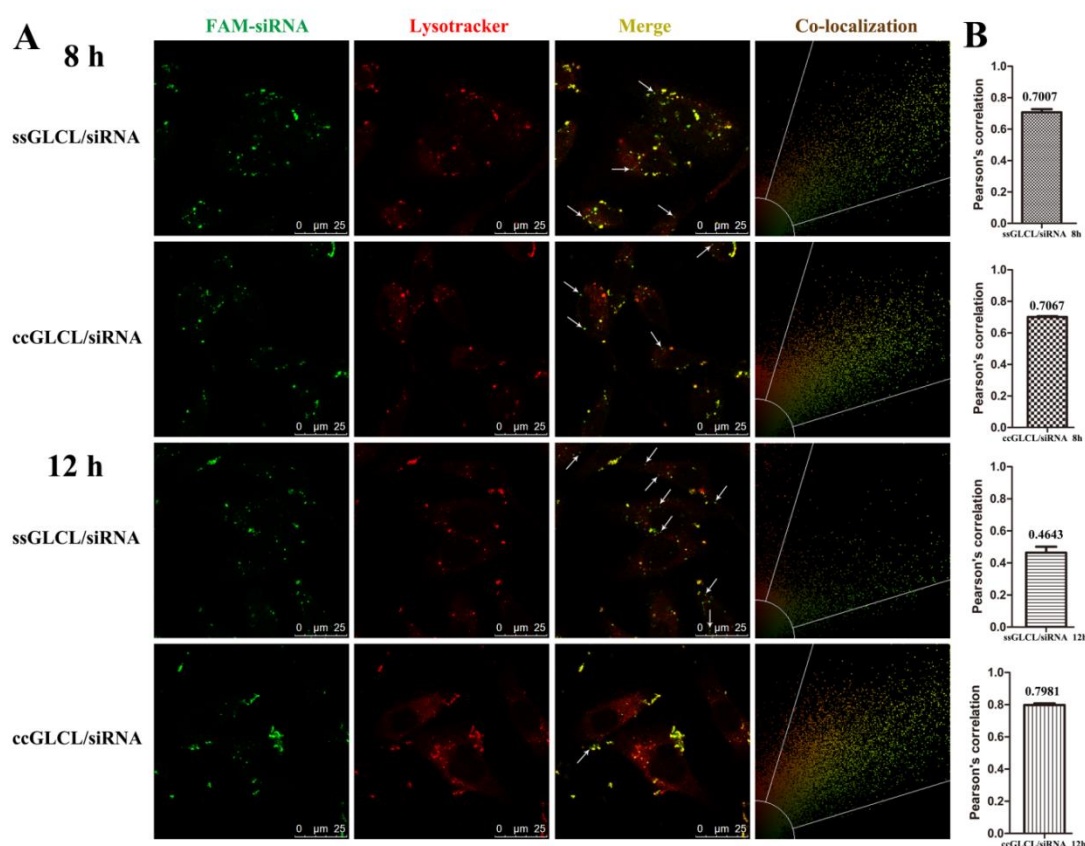


Figure 7. (A) CLSM images of MCF-7 cells after incubation with **ssGLCL/siRNA** nanoplexes and **ccGLCL/siRNA** nanoplexes at N/P = 10/1 for 8 h and 12 h periods. The Lysotracker Red DND-99 (red) was used to stain endosomes/lysosomes. The final FAM-siRNA concentration is 100 nM. (B) The quantitative analysis of Pearson's correlation

coefficient was performed by the co-localization computation module of Leica SP8 confocal microscopy. Data was given as mean \pm SD (n = 3).

3.6 In Vitro Gene Silencing Effects.

The levels of EGFR mRNA in MCF-7 cells were detected by RT-PCR analysis after transfected with GLCL/siEGFR nanoplexes (**Figure 8A**). It was shown that both **ccGLCL/siEGFR** and **ssGLCL/siEGFR** nanoplexes could significantly knock down EGFR mRNA effectively as lipofectamine 2000, even though **ssGLCL/siRNA** showed a much lower cellular uptake than **ccGLCL/siRNA** in MCF-7 cells. Meanwhile, the control GLCL/siNC nanoplexes barely had any efficacy. These effects on mRNA level were perfect accordance with the results of EGFR protein expression in western-blot assay (**Figure 8B**). Nevertheless, a significant higher GFP silencing effect was observed in **ssGLCL/siGFP** nanoplexes when compared to that of **ccGLCL/siGFP** nanoplexes (**Figure 8C**). It was worthy to mention that the same results of cellular uptake were found in HeLa cells after treated with these two GLCL/siRNA nanoplexes.

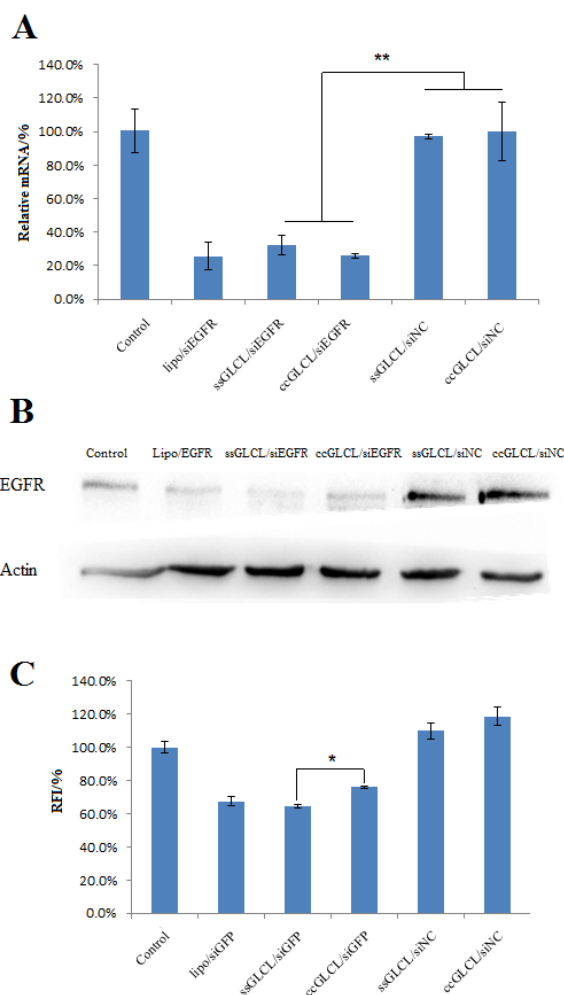


Figure 8. Relative levels of EGFR mRNA in MCF-7 detected by RT-PCR analysis (A), EGFR protein expression detected by Western-blot assay (B), relative fluorescence intensity (RFI) in GFP-HeLa cells detected by flow cytometry (C), after transfection of different nanoplexes

with a final siRNA concentration of 100 nM at the N/P ratio of 10/1. Data was shown as mean \pm SD (n=3). ** p < 0.01, * p < 0.05.

To further confirm the concentration-dependent gene silencing efficiency, the levels of VEGF protein expression in cell culture medium were detected by using a Human VEGF immunoassay kit after the cells transfected with various nanoplexes (N/P ratio was 10/1) containing different concentrations of siRNA (30 nM, 50 nM, 100 nM), respectively. From the results in **Figure 9**, it was shown that VEGF protein could be significantly knocked down by siVEGF at three concentrations in both MCF-7 and HeLa cells. When the final siVEGF concentration was 100 nM (**Figure 9C**) or 50 nM (**Figure 9B**), a similar silencing activity on VEGF was observed between **ssGLCL/siRNA** nanoplexes and **ccGLCL/siRNA** nanoplexes. While at the siVEGF concentration of 30 nM (**Figure 9A**), **ssGLCL/siRNA** nanoplexes displayed a significantly higher inhibition effects on targeted VEGF protein in both HeLa cells and MCF-7 cells than **ccGLCL/siRNA** nanoplexes (P < 0.01).

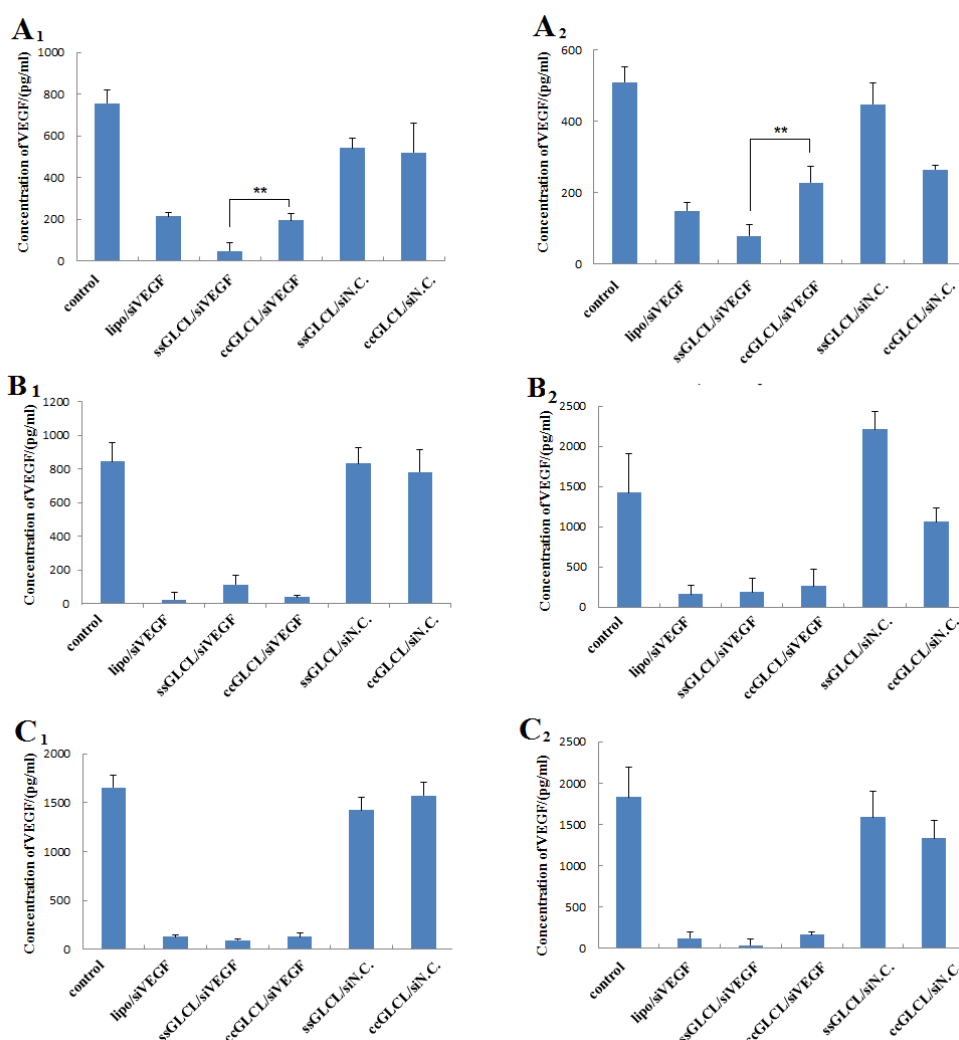


Figure 9. Concentration-dependent gene silencing effects on VEGF expression. The levels of VEGF expression in culture medium were detected by Elisa VEGF kit after transfected with different nanoparticles in MCF-7 cells (1) and HeLa cells (2). The final siRNA concentration

of siRNA was 30 nM (A), 50 nM (B), 100 nM (C), respectively. N/P ratio was 10/1. Data was shown as mean \pm SD (n = 3). **p < 0.01.

3.7 *In vivo* Anti-Tumor Study.

Nude mice xenografted with human breast MCF-7 tumor were injected intratumorally for a total of four treatments at the days indicated as arrows in **Figure 10A**. After inoculation, tumor growth inhibition efficacy was calculated from the changes of tumor size after intratumorally administration of different siRNA formulations, and 5% glucose was used as control. Both **ccGLCL/siEGFR** nanoplexes and **ssGLCL/siEGFR** nanoplexes exhibited significantly higher tumor growth inhibition effects than **GLCL/siNC** nanoplexes, through intratumoral injection after injection for 3 doses ($P < 0.05$). However, there was no significant difference of tumor growth inhibition effects between **ccGLCL/siEGFR** nanoplexes and **ssGLCL/siEGFR** nanoplexes. The *in vivo* antitumor efficacies of these two formulations were consistent with the *in vitro* gene silencing effects very well. The body weight was measured every day for safety evaluation. As shown in **Figure 10B**, there was no significant change of body weight in all of mice during the whole experimental period, as similar as that of 5% glucose group.

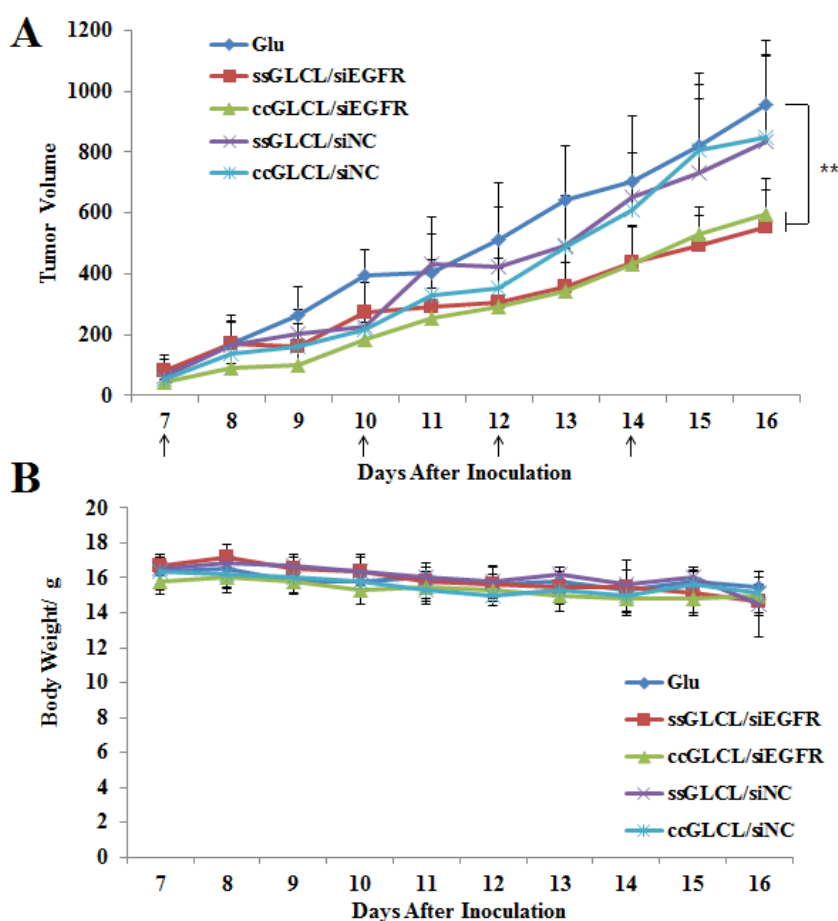


Figure 10. Anti-tumor effects of various nanoplexes. Female Balb/c nude mice xenografted MCF-7 tumors were injected intratumorally with different siRNA complexes (each dose of 1 mg siRNA/kg) for a total of 4 doses at the day indicated as arrows. A. The changes of tumor

size after treated with GLCL/siRNA nanoplexes. B. The changes of body weight. (** $p < 0.01$)

3.8 Immunofluorescence Detection of EGFR Protein in Tumor Tissues.

As seen from **Figure 11**, both **ssGLCL/siEGFR** and **ccGLCL/EGFR** group showed thorough down-regulation of EGFR protein which stained as green by FITC-labeled EGFR antibody, while siNC groups had no such effect. These results indicated that both **ssGLCL/siEGFR** nanoplexes and **ccGLCL** ones exhibited the efficient antitumor activity with a gene sequence-specific pattern.

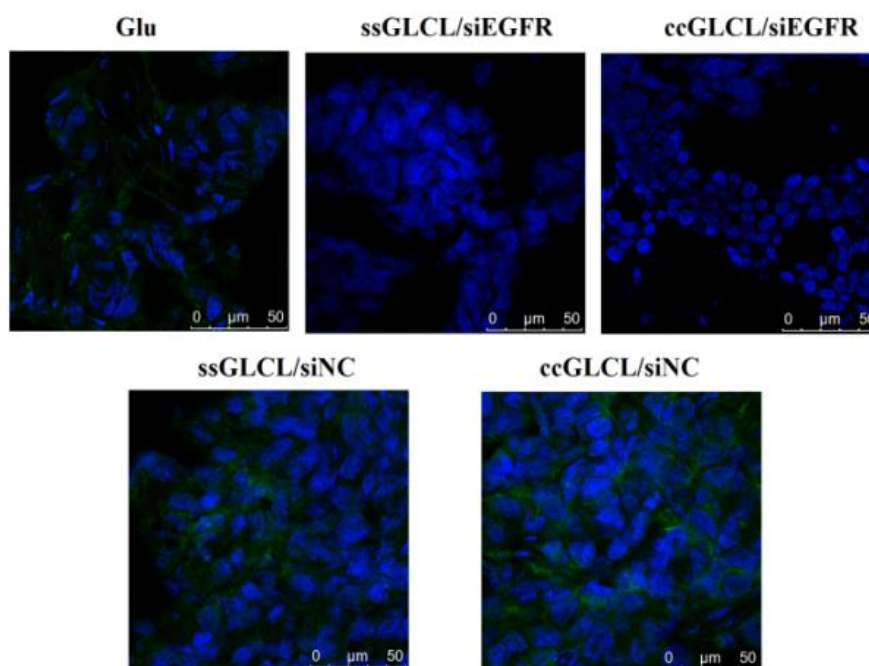
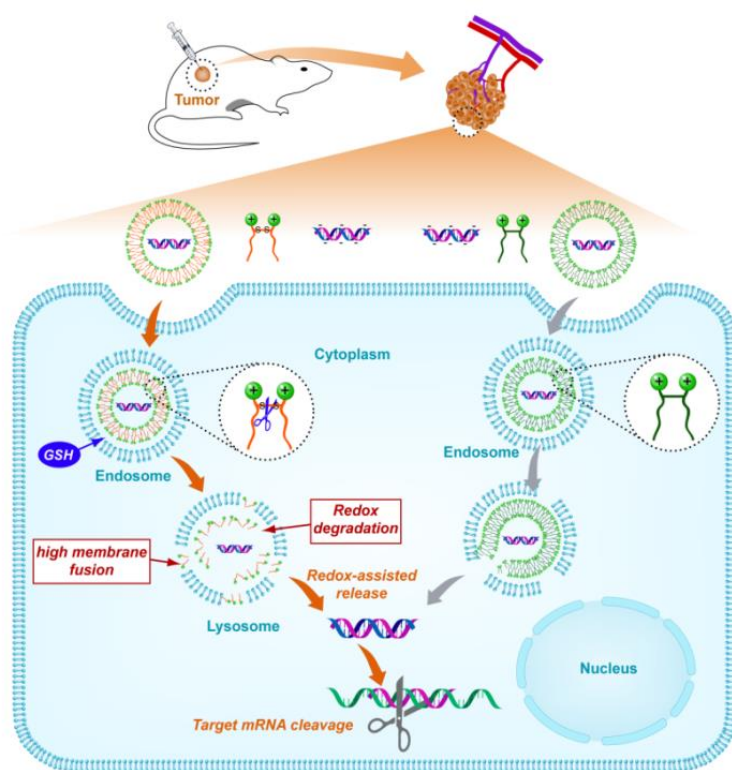


Figure 11. Immunofluorescence detection of EGFR expression in tumor tissue cryo-sections by confocal microscopy. Green color represents for EGFR binding with FITC-labeled antibody, and blue color represents for nuclei stained with Hoechst 33258.

4. Discussions.

With greater understanding of the difference between normal and pathological tissues and cells, temperature, pH, enzyme and hypoxia are examples of "triggers" at the diseased site that could be exploited with stimuli-responsive nanocarriers. A nanocarrier system incorporated with stimuli-responsive property (e.g. pH or redox potential) would be used to overcome some of the systemic and intracellular delivery barriers [23-27].

In the current study, we incorporated disulfide (-S-S-) linkage into the H-shape structure of gemini-like cationic lipid to make the gemini lipid biodegradable as well. Here we presented for the first time the transfection properties of this comparable non-reducible **ccGLCLs** and elucidated the role of disulfide-bridge on the activity of redox-response **ssGLCL/siRNA** nanoplexes in different cell lines (cervical cancer HeLa cell line and breast cancer MCF-7 cell line) (**Scheme 2**). Transfection activities have been performed with three kinds of siRNA sequences targeted EGFR, VEGF and GFP, respectively.



Scheme 2 Schematic illustration of the redox-assisted release of siRNA from **ssGLCL** nanoplexes compared to that of **ccGLCL** nanoplexes. The GLCL/siRNA nanoplexes were prepared with electrostatic interaction. After cell internalization, the **ssGLCLs** were split into two single chain lipid units with the cleavage of disulfide-bridge by abundant reductive glutathione (GSH) in cells, then the resulted monomeric lipid unit exhibited higher membrane fusion and facilitated release of siRNA from lysosomes into cytoplasm, thus an enhanced gene silencing effects on targeted mRNA was obtained.

Biosafety and gene silencing activity are the two essential requirements of nanocarriers applied for gene delivery [33-35]. As reported in previous studies, gemini-like cationic lipid, comprising a dimeric form of two symmetrical monomeric lipid units via a suitable linker, exhibited not only higher encapsulation efficiency but also lower cytotoxicity than those corresponding monomeric lipid units, which displayed advantages for delivery DNA and antisense oligonucleotide (AS-ODN) drugs [17-19]. In our study, it was demonstrated that both two H-shape gemini cationic lipids (**ssGLCLs** and **ccGLCLs**) could individually self-assemble into cationic nanoparticles in water phase and compact negatively-charged siRNA into nanoplexes with particle size of ~ 200 nm and zeta potential of $\sim +30$ mV (**Table 1** and **Figure 2**). Gel retardation assay also displayed both GLCL nanoparticles exhibited high encapsulation efficiency of siRNA even at the N/P ratio of 3/1 (**Figure 3A**). Compared to monomeric lipid unit **sGLCLs**, both **ssGLCLs** and **ccGLCLs** showed significantly lower cytotoxicity in MCF-7 cells (**Figure 3B**). Furthermore, *in vitro* and *in vivo* gene silencing experiments confirmed both **ssGLCL/siRNA** nanoplexes and **ccGLCL/siRNA** nanoplexes could exhibit a high cellular uptake and the sequence-specific down-regulation effects on targeted mRNA and protein expression, verified by RT-PCR analysis, western-blot assay and

in vivo tumor growth inhibition (**Figure 8-11**). All above results demonstrated that both two H-shape GLCLs-based systems would be potential carriers towards improving siRNA delivery. Furthermore, it was revealed that the internalization pathway of **ssGLCLs** nanoplexes and **ccGLCLs** nanoplexes were predominantly dependent on the CME-mediated endocytosis (**Figure 5**), and there was no significant difference between **ssGLCLs** and **ccGLCLs** found in both MCF-7 cells and HeLa cells.

Surprisingly, an unexpected outcome of gene silencing efficacy was observed in **ssGLCLs**, in comparison with **ccGLCLs**. During *in vitro* gene silencing experiments, it was displayed that the **ssGLCL/siEGFR** nanoplexes exhibited similar down-regulation effects on both levels of EGFR mRNA and proteins expression when compared to the **ccGLCL/siRNA** nanoplexes (**Figure 8A and 8B**), although a significantly lower cellular uptake of siRNA was found in the human breast cancer MCF-7 cells treated with **ssGLCLs** (**Figure 4A and 4C**). Interestingly, although a similar cellular uptake was found in GFP-HeLa cells (**Figure 4B**), the **ssGLCL/siGFP** nanoplexes showed significantly higher down-regulation effects on GFP expression compared to that of **ccGLCL/siRNA** nanoplexes (**Figure 8C**). Moreover, the **ssGLCL/siRNA** nanoplexes displayed a significantly higher inhibition effects on targeted VEGF protein in both HeLa cells and MCF-7 cells than **ccGLCL/siRNA** nanoplexes ($P < 0.01$) at the siVEGF concentration of 30 nM (**Figure 9A**). These evidences demonstrated that the **ssGLCL/siRNA** nanoplexes exhibited stronger down-regulation effects on the levels of targeted mRNA and/or proteins expression in cells, although similar or even lower cellular uptake of siRNA was found in **ssGLCLs** when compared to those of **ccGLCL/siRNA** nanoplexes. Why this phenomenon happened? What happened during transfection of **ssGLCL/siRNA** nanoplexes?

Obviously, this interesting story most likely occurred in the intracellular trafficking process. The role of reducible disulfide-bridge in **ssGLCLs** might be a key point for its higher gene silencing efficacy in comparison with **ccGLCLs**. The mechanism was hypothesized as follow: after cellular uptake of nanoplexes, the **ssGLCL** was broken into monomeric lipid units (**sGLCL**) with the cleavage of disulfide-bridge by reductive substances glutathione (GSH) [36, 37], which provided a reductive intracellular environment [38,39]; then the single chain **sGLCL** exhibited a high membrane fusion and induced further disassembly of nanoplexes. With a promoted siRNA escaping from lysosomes into cytosol, the enhanced gene silencing effects on target mRNA occurred consequently. This hypothesis was confirmed in our experiments. As seen in CLSM images (**Figure 6B and Figure 7**), at 4 h time point, **ssGLCL/FAM-siRNA** nanoplexes and **ccGLCL/FAM-siRNA** nanoplexes were all internalized into cytoplasm as green discrete dots after 4h incubation in cells. With the prolonged incubation time, the co-localization of nanoplexes and endosome/lysosomes was gradually presented as yellow dots. At 8 h or 12 h time point, much more green dots appeared again in **ssGLCL/FAM-siRNA** group, that meant large percentage of green-fluorescence labeled siRNA were released from lysosomes into cytoplasm. While the **ccGLCL/FAM-siRNA** group still displayed yellow dots mostly. It was suggested that the cleavage of disulfide-bond in lysosomes could promote the release of siRNA from **ssGLCL** nanoplexes into cytoplasm and initiation gene silencing activities.

To further elucidate the mechanisms of enhanced release of siRNA induced by biodegradation of **ssGLCLs**, we performed a hemolysis assay to mimic the enhanced

membrane fusion based on the cleavage of disulfide-bond (**Figure 6A**). 1,4-dithio-D,L-threitol (DTT) was selected as a reductive reagent in *in vitro* environment [40]. It was observed that a significant hemolysis effect (up to almost 40%) was found in **ssGLCL** nanoparticles after addition of DTT reagent, while **ccGLCL** still did not show any hemolysis effect. This significant enhancement of hemolysis effect in **ssGLCL** was probably resulted from disruption of cell membrane by the surfactant-based membrane fusion, like as the hemolysis effects (about 65%) of **sGLCL**. The rationale behind this approach was to ensure disassembling of the **ssGLCL**/siRNA complexes inside the cytoplasm after reduction of disulfide-bond by the intracellular glutathione environment. Glutathione (GSH) is an important molecule involved in the function of disulfide-bond in cells. It has been well known that a significantly high GSH concentration exists inside cells (~ 2 mM) as compared to outside cells (2 μ M) [37]. It was suggested that the vast different of GSH concentration between inside and outside could provide a potent mechanism for release of siRNA from disulfide-bridge based **ssGLCL**/siRNA nanoplexes. Therefore, we believed the difference of gene silencing efficiency between **ssGLCL** and **ccGLCL** nanoplexes was likely resulted from the special property of disulfide-bond within the reductive condition.

By insight into the mechanism of the role of disulfide-bridge in gemini like lipids, **ssGLCLs** indeed displayed its predominance of siRNA delivery *in vitro*, compared to **ccGLCLs**. Nevertheless, there was a discrepancy between *in vitro* gene silencing effects and *in vivo* anti-tumor efficiency. Although higher *in vitro* gene silencing effect and *in vivo* tumor growth inhibition were happened in **ssGLCL**/siRNA nanoplexes, no significant difference between **ssGLCLs** and **ccGLCLs** was observed in *in vivo* tumor growth inhibition (**Figure 10A**) and down-regulation of EGFR expression level (**Figure 11**). These conflicting results might be influenced from the over-dose of siRNA and the unsatisfactory administration frequency. We are progressing to meliorate the inadequacies mentioned above and will report the detail results of *in vivo* tumor therapeutic efficacy in the near future.

5. Conclusion

Based on the above mentioned mechanistic study, it was suggested that the enhanced down-regulation effects of **ssGLCL**/siRNA nanoplexes on targeted mRNA and protein expression was probably resulted from the increased release of siRNA from endosomes/lysosomes to cytoplasm, which was promoted by the enhanced lysosomal escape capacity of monomeric lipid units (**sGLCL**) after the disulfide-bridge cleavage of **ssGLCLs** in lysosomes induced by intracellular reductive substances glutathione (GSH). Therefore, we believe the redox-active disulfide bridge plays a key role on the activity of H-shape gemini-like lipid based siRNA delivery.

Acknowledgments

The authors acknowledge the financial support from the Ministry of Science and Technology of China (Grant No. 2013CB932501, 2012CB720604, 2012AA022501), the National Natural Science Foundation of China (Grant No. 81273455, 81473158 and 20932001), and Programs from Ministry of Education of China (NCET-11-0014 and BMU20110263).

References

- [1] A. Fire, S.Q. Xu, M.K. Montgomery, S.A. Kostas, S.E. Driver, C.C. Mello. Potent and specific genetic interference by double-stranded RNA in *Caenorhabditis Elegans*. *Nature*, 391(1998) 806-810.
- [2] M. Ghildiyal, P.D. Zamore. Small silencing RNAs: an expanding universe. *Nat. Genet.*, 10(2009), 94-108.
- [3] S.M. Hammond, E. Bernstein, D. Beach, G.J. Hannon. An RNA-directed nuclease mediates post-transcriptional gene silencing in *Drosophila* cells. *Nature*, 404(2000), 293-295.
- [4] Y. Dorsett, T. Tuschl. siRNA: applications in functional genomics and potential as therapeutics. *Nat. Rev. Drug Discov.*, 3(2004), 318-329.
- [5] K.A. Whitehead, R. Langer, D.G. Anderson. Knocking down barriers: advances in siRNA delivery. *Nat. Rev. Drug Discov.*, 8(2009), 129-138.
- [6] J. Wang, Z. Lu, M.G. Wientjes, J.L. Au. Delivery of siRNA therapeutics: barriers and carriers. *Aaps J.*, 12(2000), 492-503.
- [7] B.L. Davidson, P.B. Jr-McCray. Current prospects for RNA interference-based therapies. *Nat. Genet.*, 12(2011), 329-340.
- [8] H.M. Ali, G. Urbinati, M. Raouane, L. Massaad-Massade. Significance and applications of nanoparticles in siRNA delivery for cancer therapy. *Expert Rev. Clin. Pharmacol.*, 5(2012), 403-412.
- [9] P. Kesharwani, V. Gajbhiye, N.K. Jain. A review of nanocarriers for the delivery of small interfering RNA. *Biomaterials*, 33(2012), 7138-7150.
- [10] X.Z. Yang, S. Dou, Y.C. Wang, H.Y. Long, M.H. Xiong, C.Q. Mao, Y.D. Yao, J. Wang. Single-step assembly of cationic lipid polymer hybrid nanoparticles for systemic delivery of siRNA. *ACS Nano*, 6(2012), 4955-4965.
- [11] Y. Wang, L. Huang. A window onto siRNA delivery. *Nat. Biotechnol.*, 31(2013), 611-612.
- [12] B. Ozpolat, A.K. Sood, G. Lopez-Berestein. Liposomal siRNA nanocarriers for cancer therapy. *Adv. Drug Deliver. Rev.*, 66(2014), 110-116.
- [13] M. Damen, J. Aarbiou, S.F. van Dongen, R.M. Buijs-Offerman, P.P. Spijkers, M. van den Heuvel, K. Kvashnina, R.J. Nolte, B.J. Scholte, M.C. Feiters. Delivery of DNA and siRNA by novel gemini-like amphiphilic peptides. *J. Control. Release*, 145(2010), 33-39.
- [14] A.J. Kirby, P. Camilleri, J.B. Engberts, M.C. Feiters, R.J. Nolte, O. Soderman, M. Bergsma, P.C. Bell, M.L. Fielden, C.L. Garcia Rodriguez, P. Guedat, A. Kremer, C. McGregor, C. Perrin, G. Ronsin, M.C. van Eijk. Gemini surfactants: new synthetic vectors for gene transfection. *Angew. Chem. Int. Ed.*, 42(2003), 1448-1457.
- [15] S.K. Misra, M. Munoz-Ubeda, S. Datta, A.L. Barran-Berdon, C. Aicart-Ramos, P. Castro-Hartmann, P. Kondaiah, E. Junquera, S. Bhattacharya, E. Aicart. Effects of a delocalizable cation on the headgroup of gemini lipids on the lipoplex-type nanoaggregates directly formed from plasmid DNA. *Biomacromolecules*, 14(2013), 3951-3963.
- [16] J. Biswas, A. Bajaj, S. Bhattacharya. *J. Phys. Chem. B*, 115(2011), 478-486.
- [17] S. Perrone, M. Usai, P. Lazzari, S.J. Tucker, H.M. Wallace, M. Zanda. Efficient cell transfection with melamine-based gemini surfactants. *Bioconjugate Chem.* 24(2013), 176-187.
- [18] C. Bombelli, F. Faggioli, P. Luciani, G. Mancini, M.G. Sacco. Efficient transfection of

DNA by liposomes formulated with cationic gemini amphiphiles. *J. Med. Chem.*, 48(2005), 5378-5382.

[19] M. Munoz-Ubeda, S.K. Misra, A.L. Barran-Berdon, S. Datta, C. Aicart-Ramos, P. Castro-Hartmann, P. Kondaiah, E. Junquera, S. Bhattacharya, E. Aicart. How does the spacer length of cationic gemini lipids influence the lipoplex formation with plasmid DNA? Physicochemical and biochemical characterizations and their relevance in gene therapy. *Biomacromolecules*, 13(2012), 3926-3937.

[20] Y. Zheng, Y.J. Guo, Y.T. Li, Y. Wu, L.H. Zhang, Z.J. Yang. A novel gemini-like cationic lipid for the efficient delivery of siRNA. *New J. Chem.*, 38(2014), 4952-4962.

[21] D. Ma. Enhancing endosomal escape for nanoparticle mediated siRNA delivery. *Nanoscale*, 6(2014), 6415-6425.

[22] T. Sun, Y.S. Zhang, B. Pang, D.C. Hyun, M. Yang, Y.N. Xia. Engineered nanoparticles for drug delivery in cancer therapy. *Angew. Chem. Int. Ed.*, 53(2014), 12320-12364.

[23] Y. Sato, H. Hatakeyama, Y. Sakurai, M. Hyodo, H. Akita, H. Harashima. A pH-sensitive cationic lipid facilitates the delivery of liposomal siRNA and gene silencing activity in vitro and in vivo. *J. Control. Release*, 163(2012), 267-276.

[24] L. Zhu, F. Perche, T. Wang, V.P. Torchilin. Matrix metalloproteinase 2-sensitive multifunctional polymeric micelles for tumor-specific co-delivery of siRNA and hydrophobic drugs. *Biomaterials*, 35(2014), 4213-4222.

[25] J. Beloor, C.S. Choi, H.Y. Nam, M. Park, S.H. Kim, A. Jackson, K.Y. Lee, S.W. Kim, P. Kumar, S.K. Lee. Arginine-grafted biodegradable polymer for the systemic delivery of therapeutic siRNA. *Biomaterials*, 33(2012), 1640-1650.

[26] F. Perche, S. Biswas, T. Wang, L. Zhu, V.P. Torchilin. Hypoxia-targeted siRNA delivery. *Angew. Chem. Int. Ed.*, 53(2014), 3362-3366.

[27] G. Saito, J.A. Swanson, K.D. Lee. Drug delivery strategy utilizing conjugation via reversible disulfide linkages: role and site of cellular reducing activities. *Adv. Drug Deliver. Rev.*, 55(2003), 119-125.

[28] C.J. Chen, J.C. Wang, E.Y. Zhao, L.Y. Gao, Q. Feng, X.Y. Liu, Z.X. Zhao, X.F. Ma, W.J. Hou, L.R. Zhang, W.L. Lu, Q. Zhang. Self-assembly cationic nanoparticles based on cholesterol-grafted bioreducible poly(amidoamine) for siRNA delivery. *Biomaterials*, 34(2013), 5303-5316.

[29] A. Fraix, T. Le Gall, M. Berchel, C. Denis, P. Lehn, T. Montier, P.A. Jaffres. Cationic lipophosphoramidates with two disulfide motifs: synthesis, behaviour in reductive media and gene transfection activity. *Org. Biomol. Chem.*, 11(2013), 1650-1658.

[30] L. Brulisauer, N. Kathriner, M. Prenrecaj, M.A. Gauthier, J.C. Leroux. Tracking the bioreduction of disulfide containing cationic dendrimers. *Angew. Chem. Int. Ed.*, 51(2012), 12454-12458.

[31] M. Oua, R.Z. Xu, S.H. Kim, D.A. Bull, S.W. Kim. A family of bioreducible poly(disulfide amine)s for gene delivery. *Biomaterials*, 30(2009), 5804-5814.

[32] V.A. Sethuraman, M.C. Lee, Y. H. Bae. A biodegradable pH-sensitive micelle system for targeting acidic solid tumors. *Pharm. Res.*, 25(2008), 657-666.

[33] Y. Kodama, S. Harauchi, S. Kawanabe, N. Ichikawa, H. Nakagawa, T. Muro, N. Higuchi, T. Nakamura, T. Kitahara, H. Sasaki. Safe and effective delivery of small interfering RNA with polymer- and liposomes-based complexes. *Biol. Pharm. Bull.*, 36(2013), 995-1001.

- [34] S.H. Lee, B.H. Chung, T.G. Park, Y.S. Nam, H. Mok. Small-interfering RNA (siRNA)-based functional micro- and nanostructures for efficient and selective gene silencing. *Accounts Chem. Res.*, 45(2012), 1014-1025.
- [35] P. Kesharwani, V. Gajbhiye, N.K. Jain. A review of nanocarriers for the delivery of small interfering RNA. *Biomaterials*, 33(2012), 7138-7150.
- [36] I. Rebrin, S. Zicker, K.J. Wedekind, I. Paetau-Robinson, L. Packera, R.S. Sohal. Effect of antioxidant-enriched diets on glutathione redox status in tissue homogenates and mitochondria of the senescence-accelerated mouse. *Free Radic. Biol. Med.*, 39(2005), 549-557.
- [37] B. Khorsand, G. Lapointe, C. Brett, J.K. Oh. Intracellular drug delivery nanocarriers of glutathione-responsive degradable block copolymers having pendant disulfide linkages. *Biomacromolecules*, 14(2013), 2103-2111.
- [38] T. Wang, D.Y. Ng, Y. Wu, J. Thomas, T. Tam-Tran, T. Weil. Bis-sulfide bioconjugates for glutathione triggered tumor responsive drug release. *Chem. Commun.*, 50(2014), 1116-1118.
- [39] M.H. Lee, Z. Yang, C.W. Lim, Y.H. Lee, S. Dongbang, C. Kang, J.S. Kim. *Chem. Rev.*, 113(2013), 5071-5109.
- [40] S. Li, Q. He, T. Chen, W. Wu, K. Lang, Z.M. Li, J.S. Li. Controlled co-delivery nanocarriers based on mixed micelles formed from cyclodextrin-conjugated and cross-linked copolymers. *Colloid. Surface B*, 123(2014), 486-492.

Table 1 Characteristics of various nanoplexes (n=3)

Nanoplexes	Particle size (d, nm)	Polydispersity index (PDI)	Zeta potential (mV)
ssGLCL/siRNA	232.1±4.2	0.14±0.07	30.5±1.8
ccGLCL/siRNA	231.7±30.1	0.27±0.10	33.3±1.5
sGLCL/siRNA	199.0±4.7	0.31±0.03	13.9±1.5

Figure Captions

Scheme 1. Synthetic procedures of three GLCL materials. Reagents and Conditions: i. Boc_2O /dioxane, KHCO_3 aq. r.t.; ii. EDC, DMAP/DCM, r.t.; iii. TFA/ CH_2Cl_2 , r.t.; iv. EDCI, HOBT, DIEA/ CH_2Cl_2 , r.t.; v. $\text{HCl}(\text{gas})/\text{EtOAc}$, r.t.

Scheme 2 Schematic illustration of the redox-assisted release of siRNA from **ssGLCL** nanoplexes compared to that of **ccGLCL** nanoplexes. The GLCL/siRNA nanoplexes were prepared with electrostatic interaction. After cell internalization, the **ssGLCLs** were split into two single-tailed **sGLCL** with the cleavage of disulfide-bridge by abundant reductive glutathione (GSH) in cells, then the resulted monomeric lipid unit exhibited higher membrane fusion and facilitated release of siRNA from lysosomes into cytoplasm, thus an enhanced gene silencing effects on targeted mRNA was obtained.

Figure 1. Structures of **ssGLCL/ccGLCL/sGLCL** materials.

Figure 2. Characterization of the prepared nanoparticles. TEM (A) and AFM (B) images of GLCL nanoparticles and their siRNA complexes. Size and zeta potential of nanoplexes detected by DLS (C).

Figure 3. Gel retardation assay for various nanoplexes at different N/P ratios (A). Cytotoxicity of various GLCL nanoparticles in MCF-7 cells (B).

Figure 4. Cellular uptake of various nanoplexes in MCF-7 cells (A) and HeLa cells (B). The intracellular fluorescence intensities were detected by flow cytometric after 4h incubation with different nanoplexes with different N/P ratios. The data was shown as mean \pm SD (n = 3). (C) Confocal laser scanning microscope images of MCF-7 after 4h incubation with **ssGLCL/siRNA** nanoplexes and **ccGLCL/siRNA** nanoplexes with a final siRNA concentration of 100 nM at N/P = 10/1. The Rhodamine-labeled phalloidin (red) was used to show the cytoskeleton and Hoechst 33258 (blue) for nucleus.

Figure 5. Internalization of various nanoplexes after treated with different inhibitors in MCF-7 cells (A) and HeLa cells (B). The intracellular fluorescence intensities were detected by flow cytometry after 4 h incubation. The mock (100%) was the fluorescence intensity of various nanoplexes without inhibitors. The data was shown as mean \pm SD (n = 3). (C) Internalization pathways of various nanoplexes in MCF-7 cells by confocal microscopy. Hoechst 33258 (Blue) and rhodamine-labeled phalloidin (Purple) were used to show the nucleus and membrane respectively. The final concentration of Cy5-labeled siRNA (Red) was 100 nM.

Figure 6. A. Relative hemolysis effects of different nanoplexes in the absence/presence of DTT with different incubation time at 37°C. Data was shown as mean \pm SD (n=3). ** p < 0.01. B. CLSM images of MCF-7 cells after incubated with various GLCL/siRNA nanoplexes at

N/P = 10/1 for different time periods. The LysolTracer Red DND-99 (red) was used to show the endosomes/lysosomes. The final FAM-siRNA concentration is 100 nM.

Figure 7. (A) CLSM images of MCF-7 cells after incubation with ssGLCL/siRNA nanoplexes and ccGLCL/siRNA nanoplexes at N/P = 10/1 for 8 h and 12 h periods. The LysolTracker Red DND-99 (red) was used to stain endosomes/lysosomes. The final FAM-siRNA concentration is 100 nM. (B) The quantitative analysis of Pearson's correlation coefficient was performed by the co-localization computation module of Leica SP8 confocal microscopy. Data was given as mean \pm SD (n = 3).

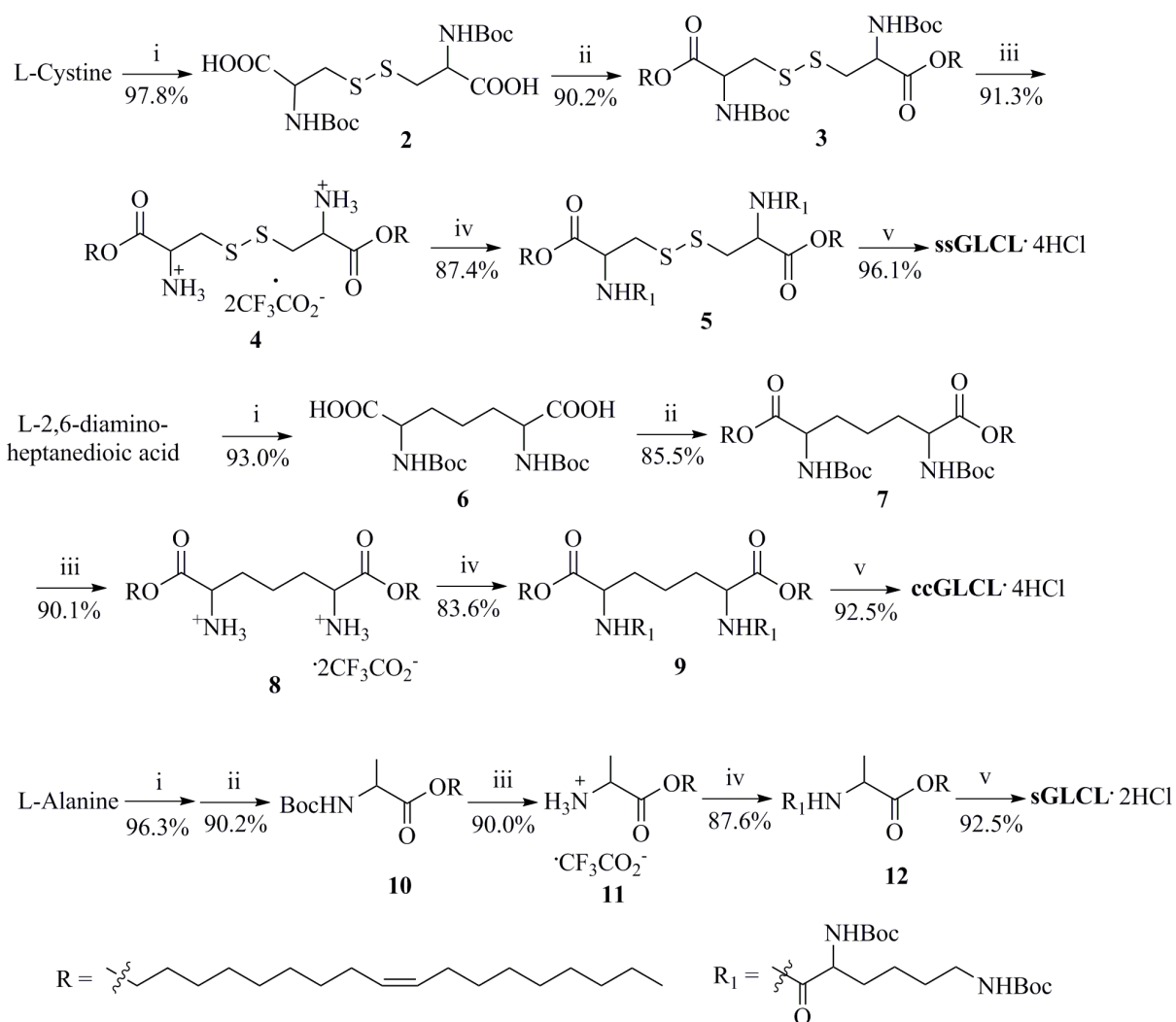
Figure 8. Relative levels of EGFR mRNA in MCF-7 detected by RT-PCR analysis (A), EGFR protein expression detected by Western-blot assay (B), relative fluorescence intensity (RFI) in GFP-HeLa cells detected by flow cytometry (C), after transfection of different nanoplexes with a final siRNA concentration of 100 nM at the N/P ratio of 10/1. Data was shown as mean \pm SD (n=3). ** p < 0.01, * p < 0.05.

Figure 9. Concentration-dependent gene silencing effects on VEGF expression. The levels of VEGF expression in culture medium were detected by Elisa VEGF kit after transfected with different nanoparticles in MCF-7 cells (1) and HeLa cells (2). The final siRNA concentration of siRNA was 30 nM (A), 50 nM (B), 100 nM (C), respectively. N/P ratio was 10/1. Data was shown as mean \pm SD (n = 3). **p < 0.01.

Figure 10. Anti-tumor effects of various nanoplexes. Female Balb/c nude mice xenografted MCF-7 tumors were injected intratumorally with different siRNA complexes (each dose of 1 mg siRNA/kg) for a total of 4 doses at the day indicated as arrows. A. The changes of tumor size after treated with GLCL/siRNA nanoplexes. B. The changes of body weight. (** p < 0.01)

Figure 11. Immunofluorescence detection of EGFR expression in tumor tissue cryo-sections by confocal microscopy. Green color represents for EGFR binding with FITC-labeled antibody, and blue color represents for nuclei stained with Hoechst 33258.

Scheme 1



Scheme 2

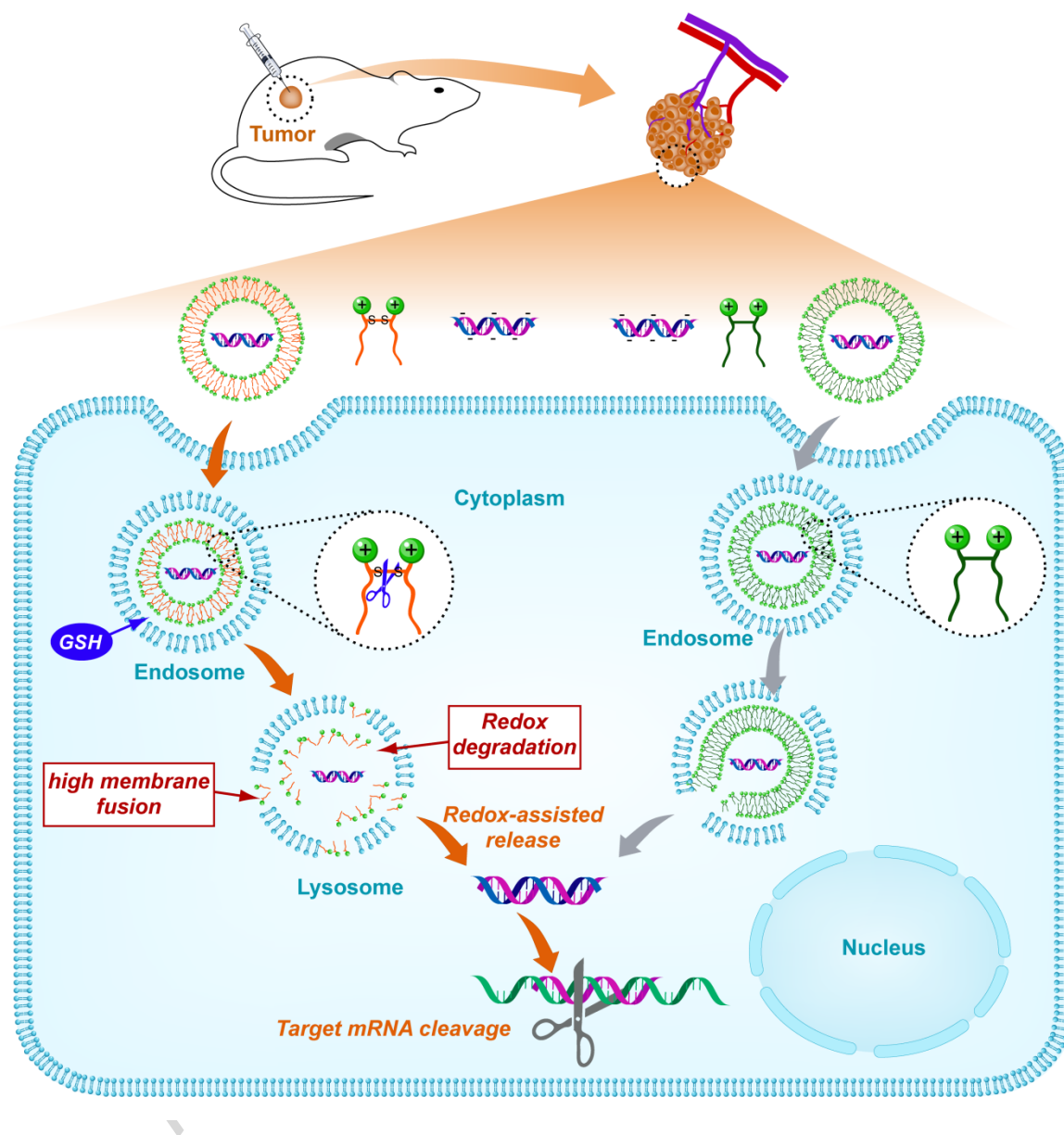


Figure 1

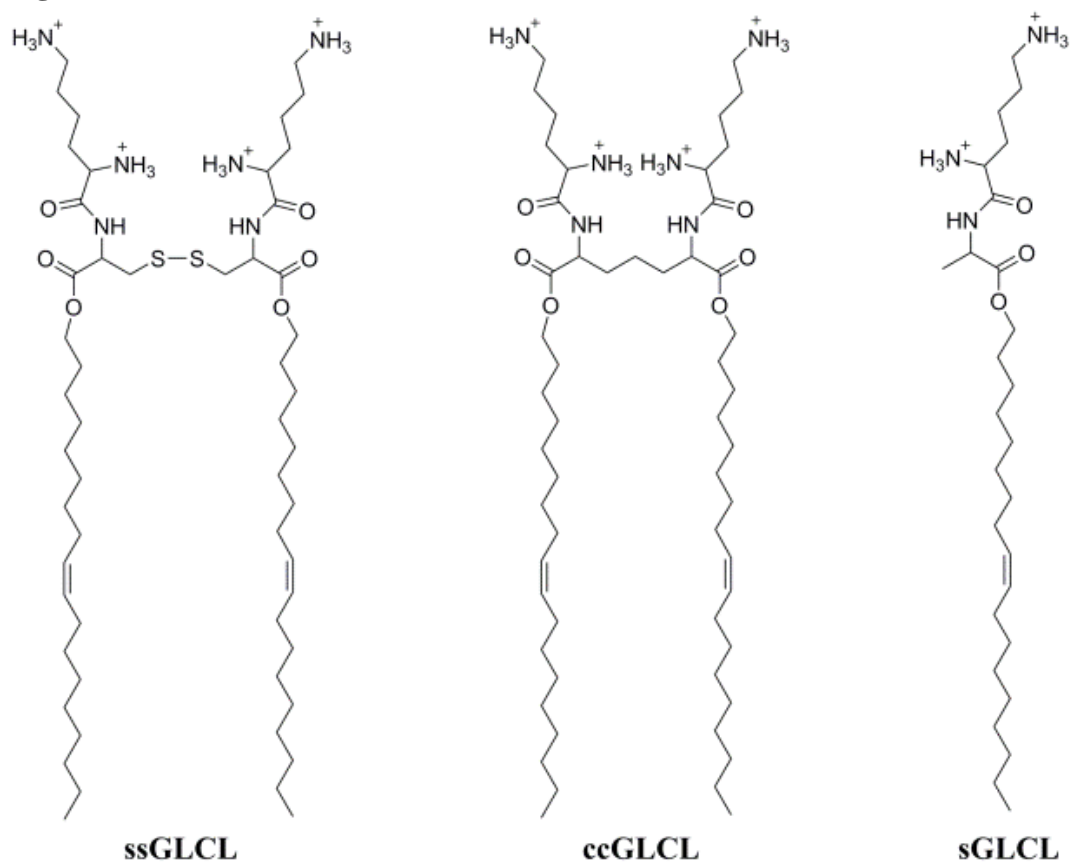


Figure 2

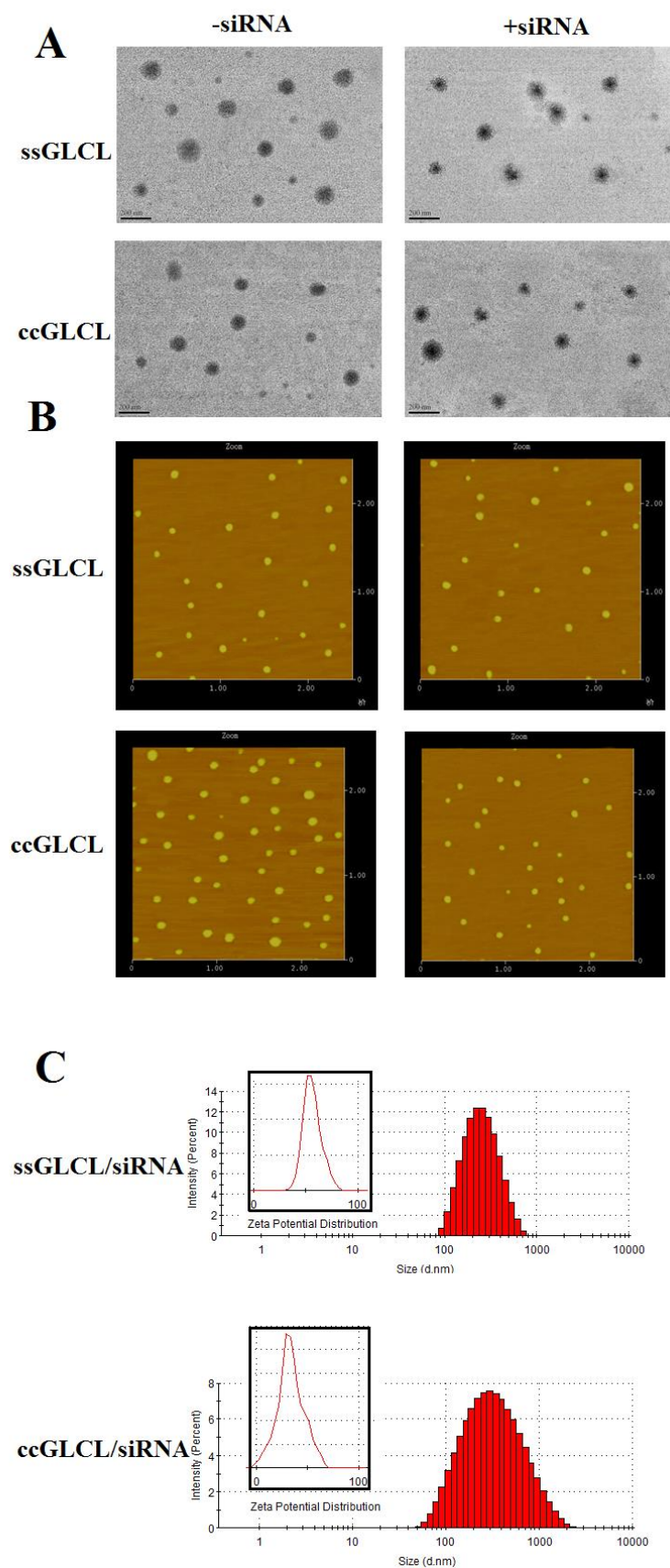


Figure 3

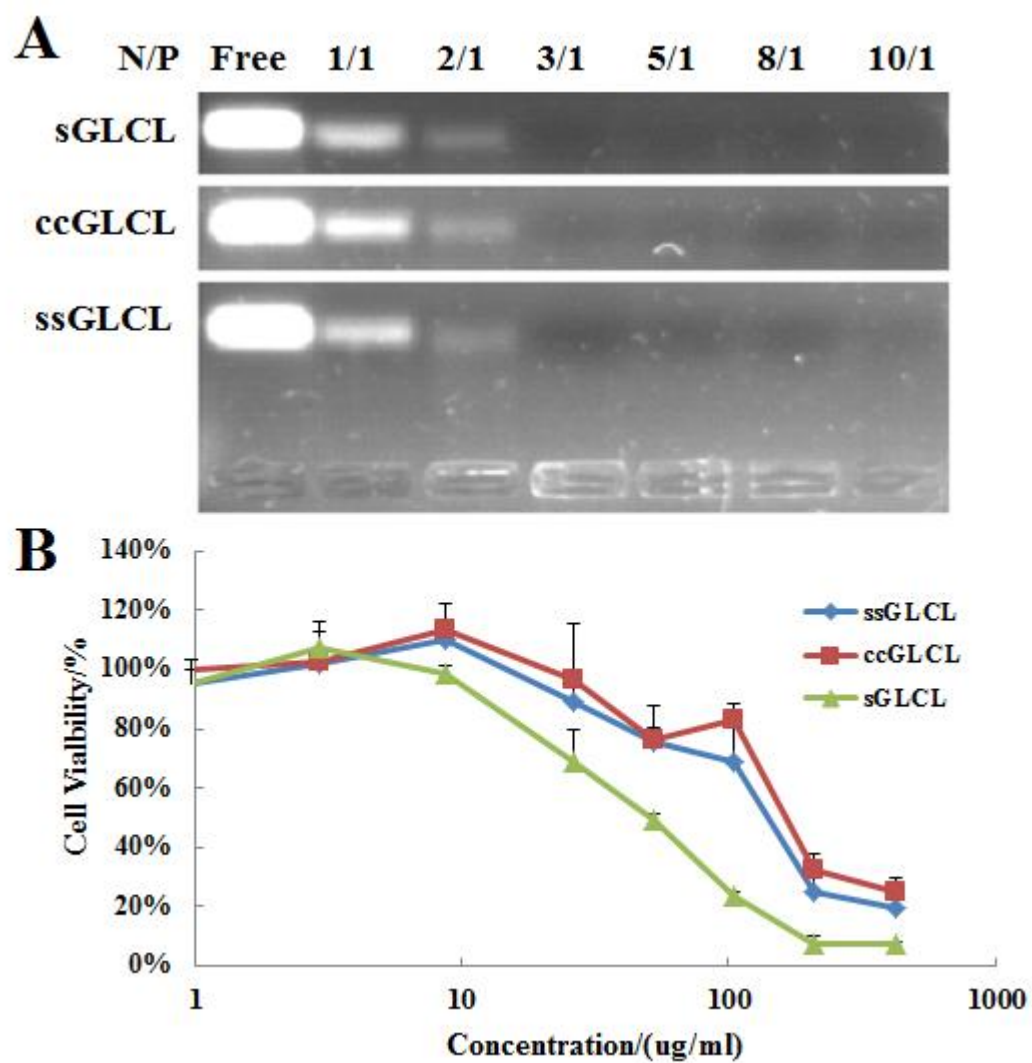


Figure 4

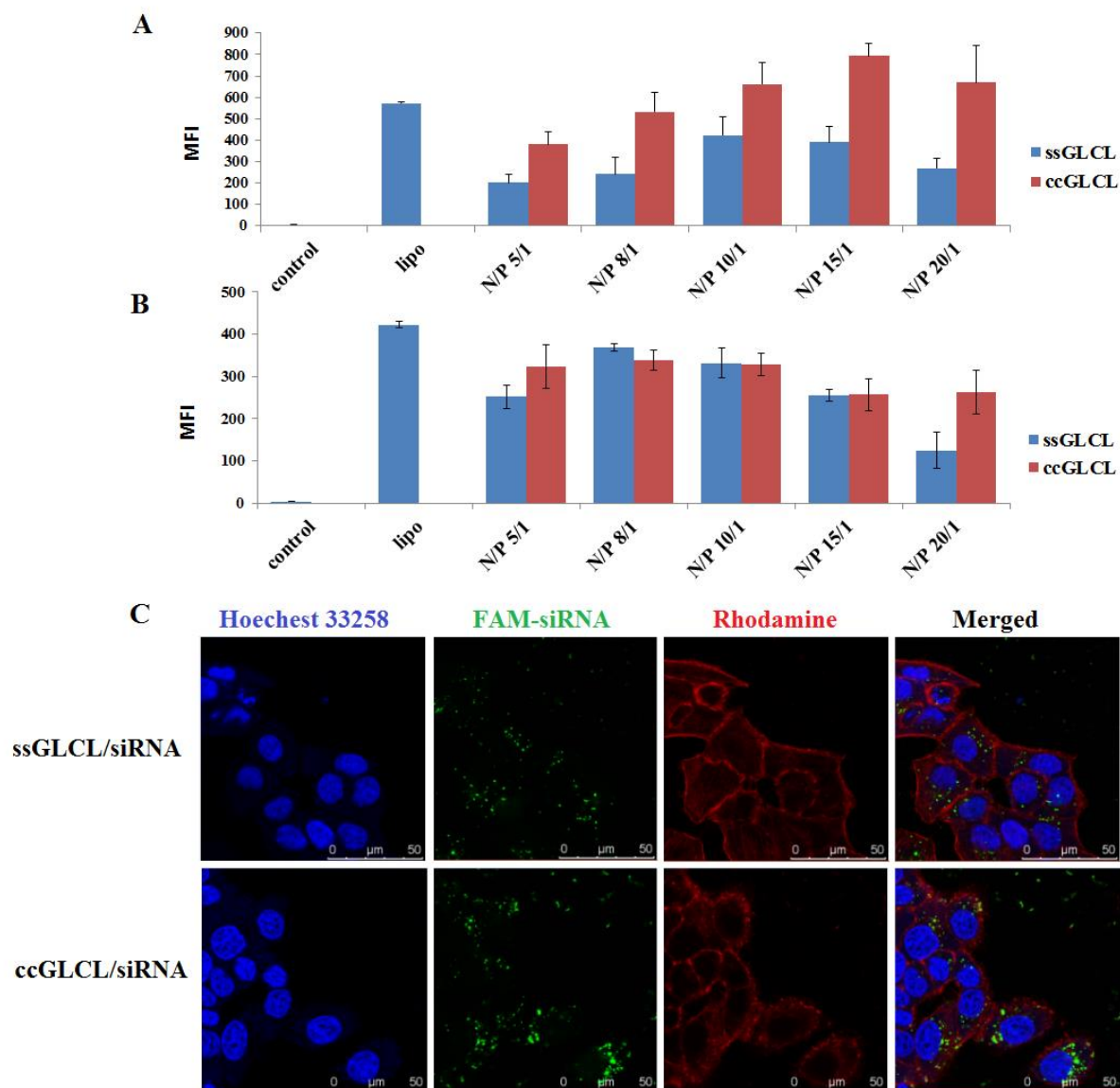


Figure 5

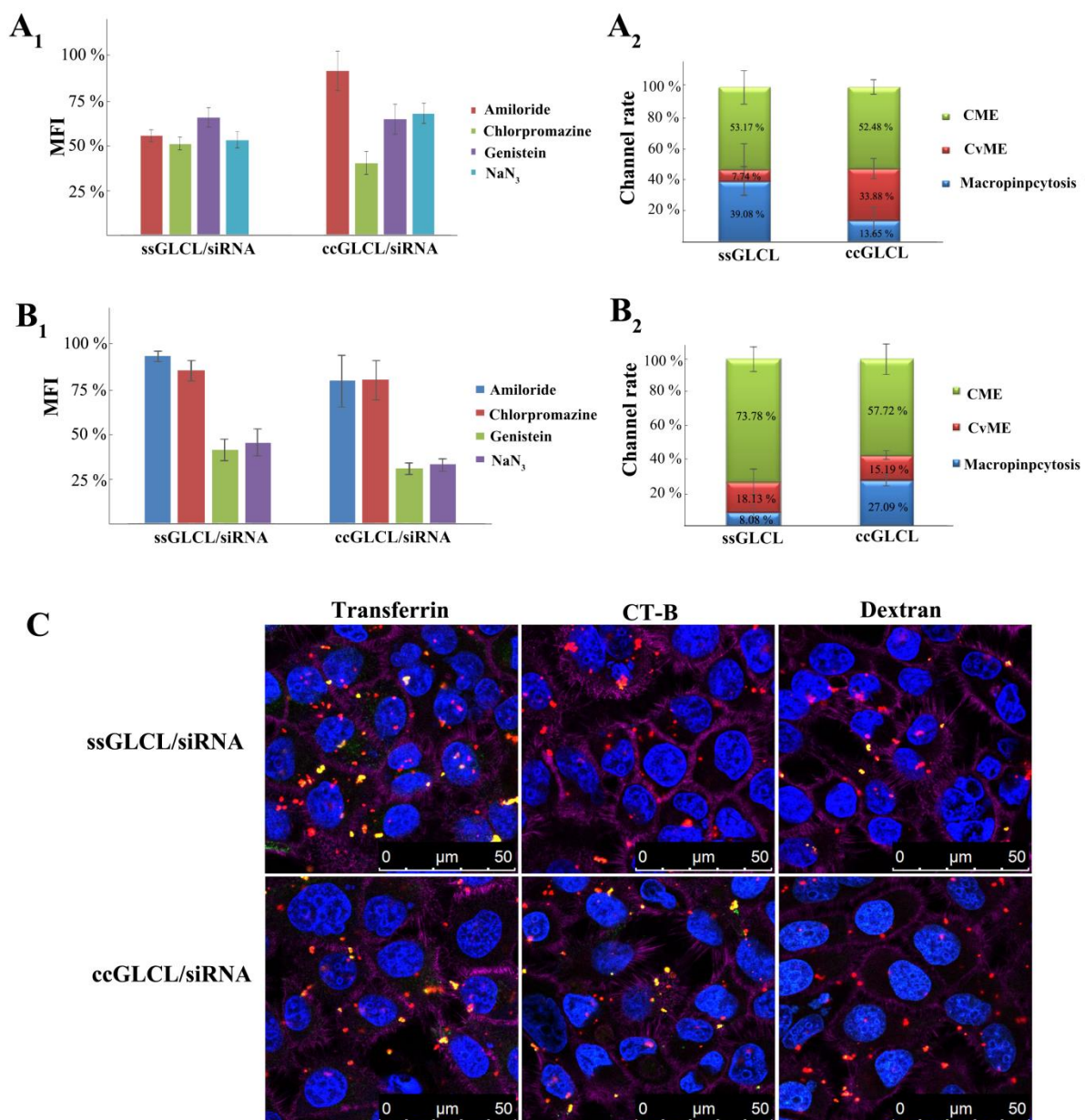


Figure 6

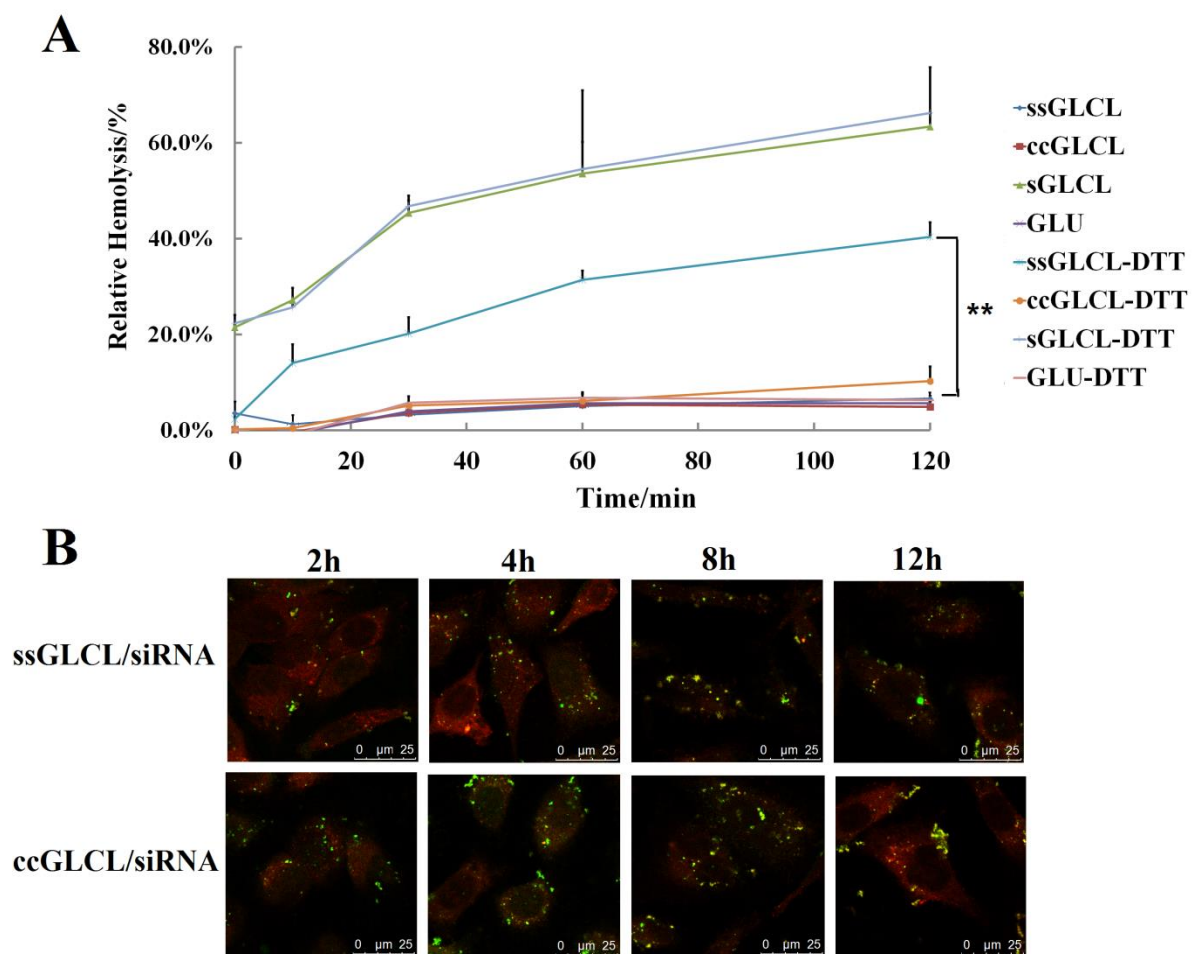
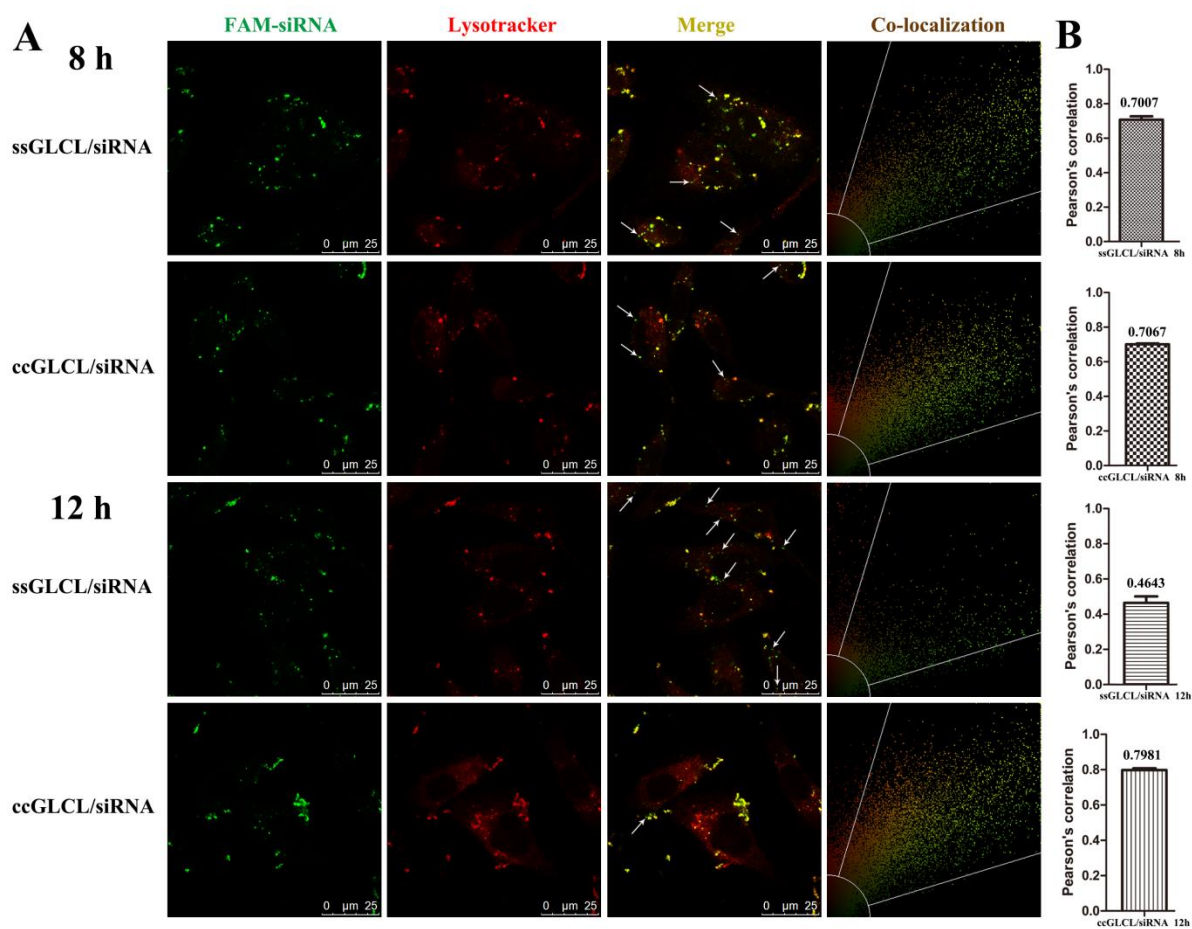


Figure 7



ACCEPTED

Figure 8

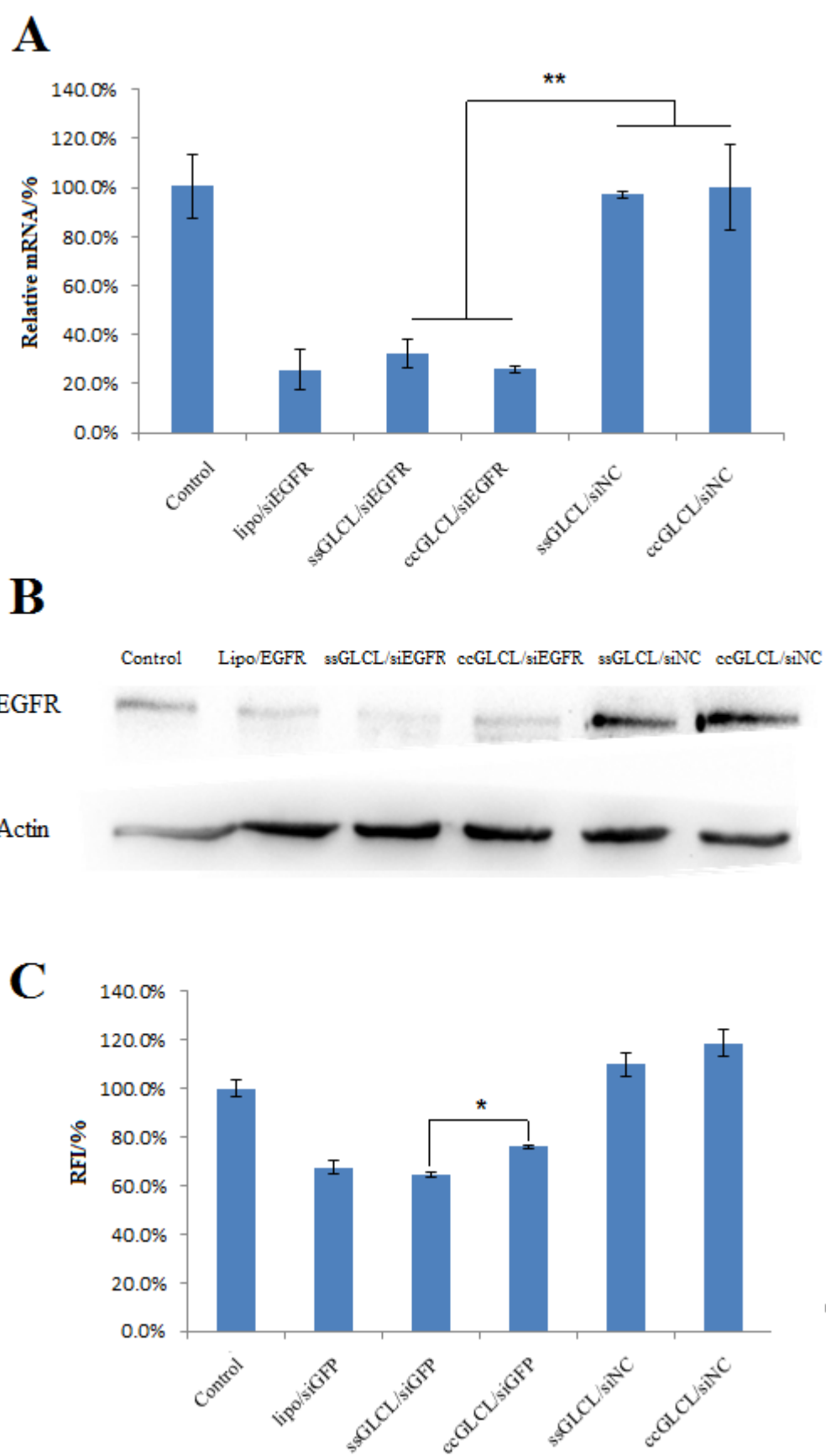


Figure 9

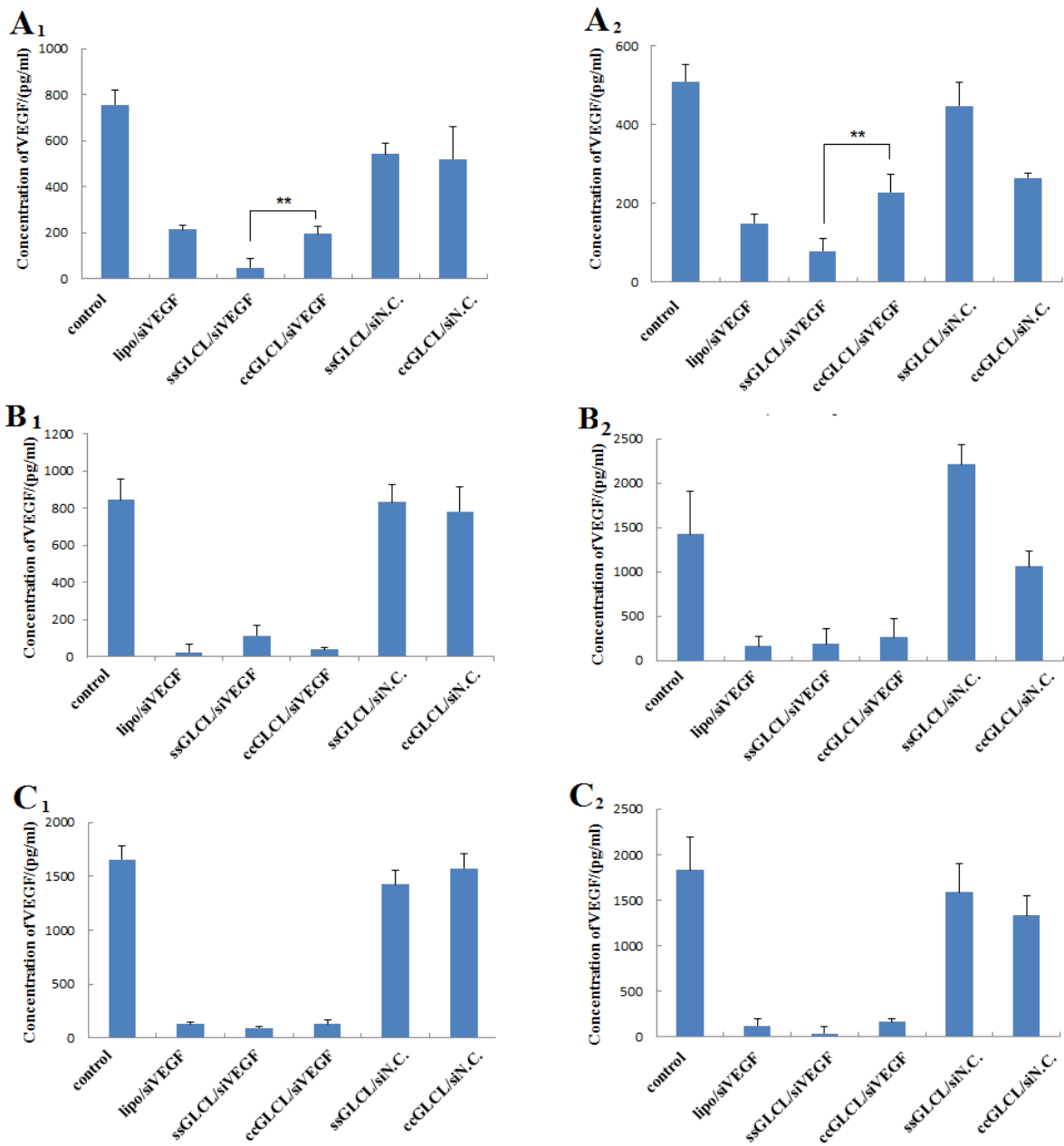


Figure 10

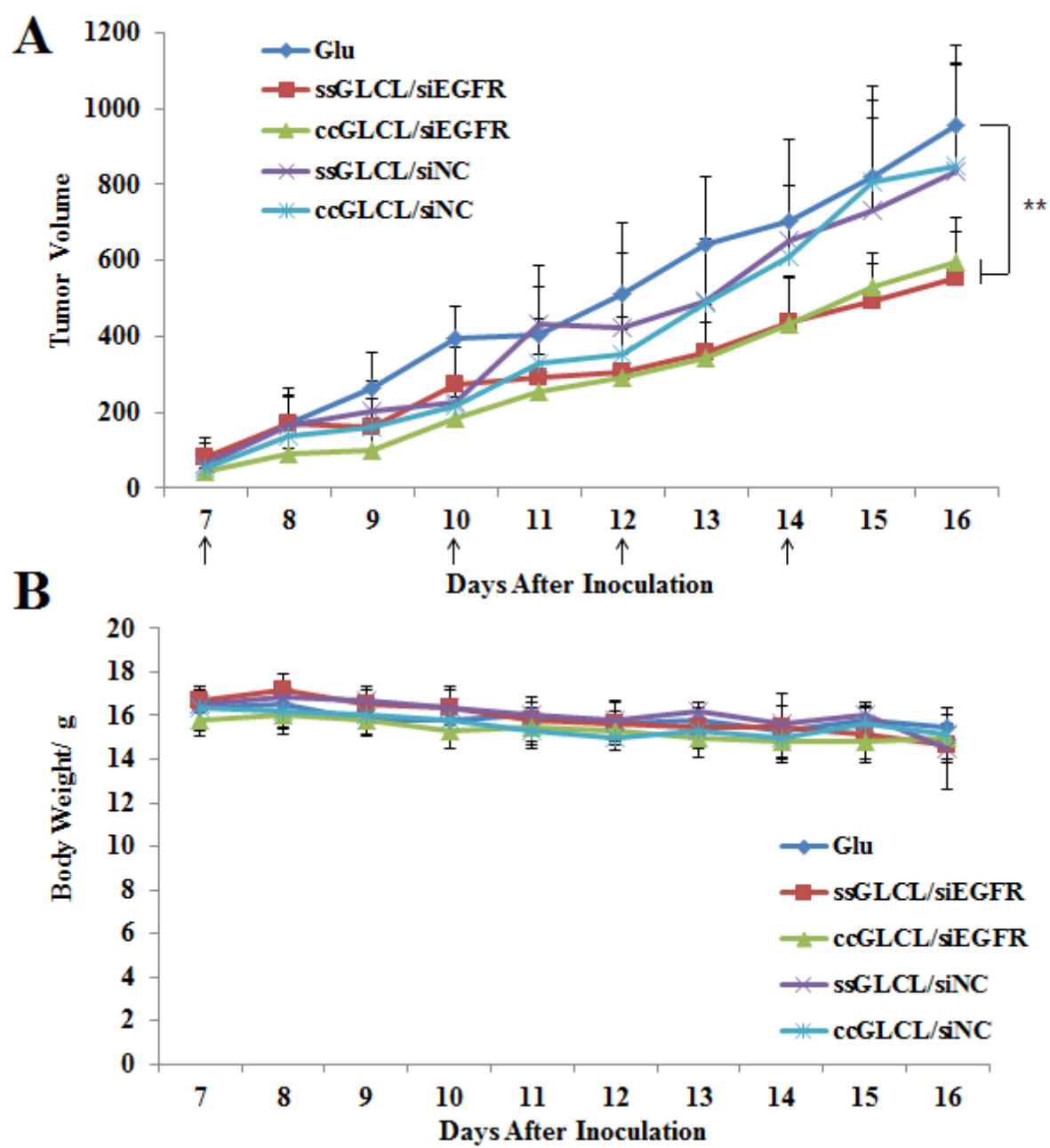
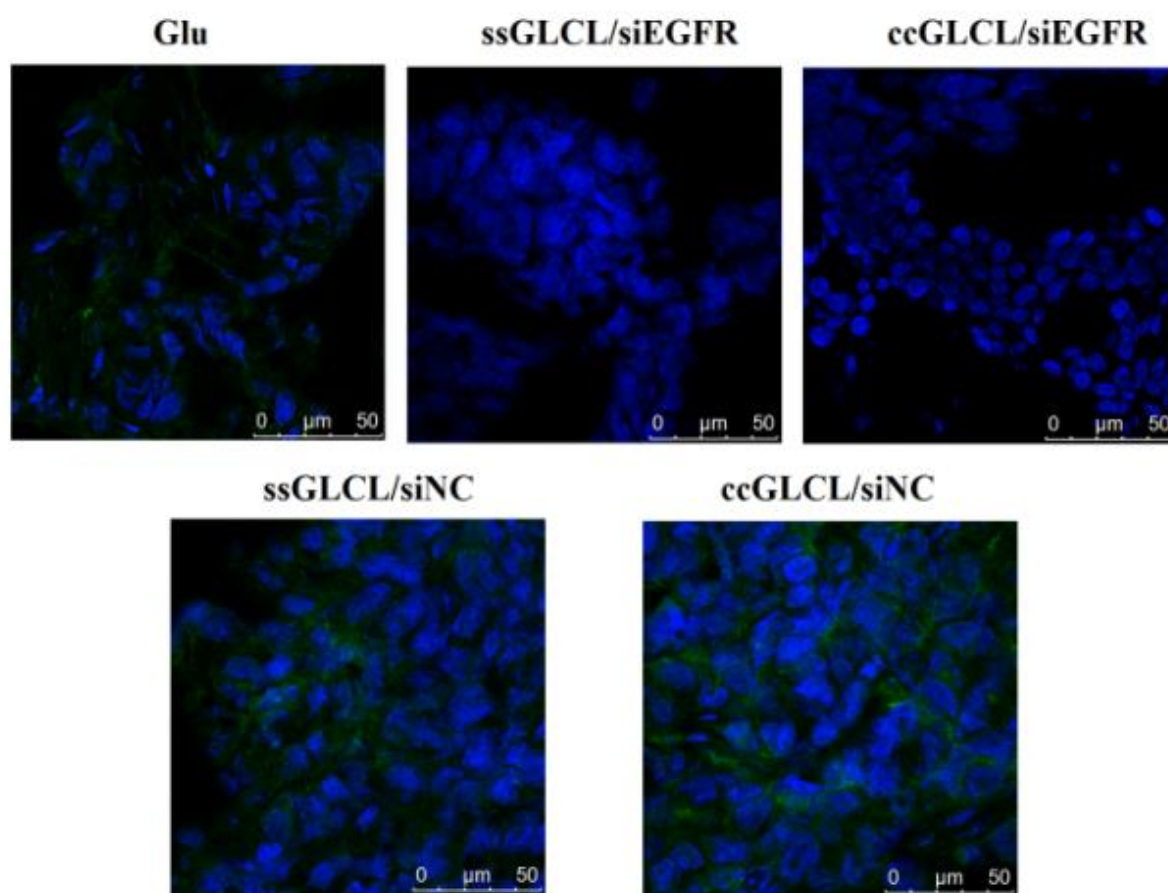
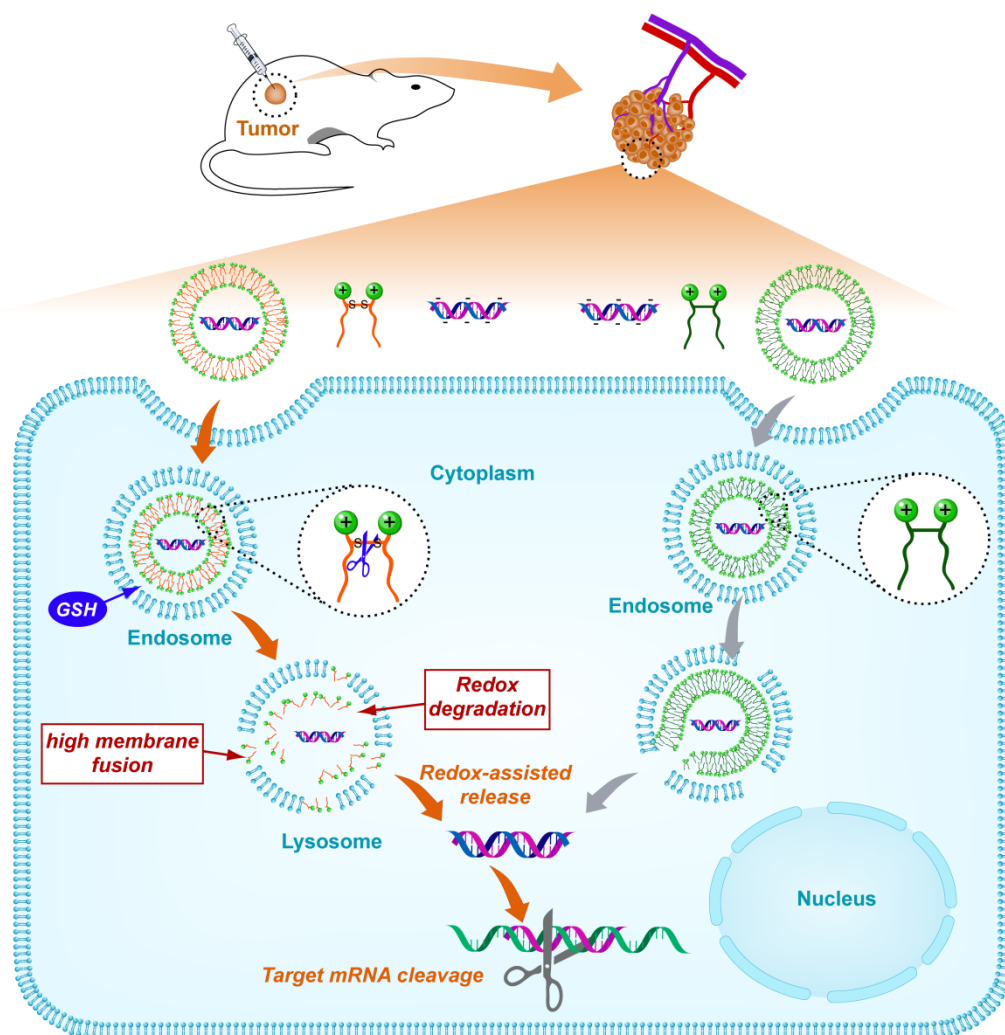


Figure 11



ACCEPTED

Graphical abstract



The GLCL/siRNA nanoplexes were prepared with electrostatic interaction. After cell internalization, the ssGLCLs were split into two single chain lipid units with the cleavage of disulfide-bridge by abundant reductive glutathione (GSH) in cells, then the resulted monomeric lipid unit exhibited higher membrane fusion and facilitated release of siRNA from lysosomes into cytoplasm, thus the enhanced gene silencing effects on targeted mRNA were obtained.